EU Fifth Framework Programme 1998-2002
Energy, Environment and Sustainable Development

Environmental Design of Low Crested Coastal Defence Structures

Deliverable 23 and 44

Report on turbulent flow velocities in the surface region of LCS

Contract n°EVK3-CT-2000-00041

EU Fifth Framework Programme 1998-2002
Energy, Environment and Sustainable Development

Environmental Design of Low Crested Coastal Defence Structures (DELOS)

Report

Deliverables D23 and D44
WP 2.3.

Report on turbulent flow velocities in the surface region of LCS

Prepared by

Inigo J. Losada, Nicolas Garcia, Javier L. Lara

Ocean & Coastal Research Group
University of Cantabria

Date of preparation: 2003-12-1 Contract: n^{o} EVK3-CT-2000-00041

Report on turbulent flow velocities in the surface region of low crested structures

Inigo J. Losada, Nicolas Garcia, Javier L. Lara

Ocean & Coastal Research Group
University of Cantabria
Dpto. de Ciencias y Técnicas del Agua y del Medio Ambiente.
E.T.S.I. de Caminos, Canales y Puertos. Avda. de los Castros s/n, 39005 Santander. Spain.

Contents

1. Introduction

Low-crested structures (hereafter LCS) are increasingly regarded by coastal engineers and planners as a valuable alternative to more classical surface-piercing and/or hard structures. By low-crested structures we mean detached rubble-mound breakwaters built with the crown elevation near the still water level. Thus, these structures may be submerged, emerged, or both alternatively, but are characterized to be strongly overtopped. The increasing interest, for aesthetic, economical and environmental reasons, towards LCS makes a better understanding of their hydrodynamics crucial. These structures are primarily designed to reduce the wave loads on the coast through a series of wave transformation processes on and inside the structure that make the wave-structure interaction modelling very complex. The relative importance of each one of the physical processes, hereafter described, that take place in the interaction of a wave train with a low-crested structure depends on the wave parameters (height, period, relative depth) and on the rubble mound characteristics (geometry, porosity, permeability).

When the incident wave train impinges on the structure, part of the energy is reflected back to the sea and part is transmitted in the leeside zone. Reflection is an important characteristic of LCS as this type of structure is generally built with relatively steep slopes. The interferences between the incident and reflected waves give rise to standing wave patterns that affect the near-field flow and subsequently the stability of the sructure. Besides, as waves shoal on the rising front of the structure, significant nonlinear effects occur, resulting in the amplification of bound waves (phase-locked with the primary wave). Most of the incident wave energy is lost on the structure's crest, essentially by breaking. Part of the energy is also dissipated by air entrainment and friction at the solid skeleton interface and within the porous media. For non-breaking waves, the flow resistance in the porous media is the main dissipation mechanism. Besides, during the breaking process, the bound waves enhanced at the shoaling stage of the propagation are released. Significant nonlinear interactions occur in the zone of the structure crest between the various wave phases and some energy is transferred from the fundamental wave frequency to higher harmonics (Driscoll *et al.*, 1993, Beji and Battjes, 1994, Losada *et al.*, 1996a, b). In the deeper waters of the

leeside zone, the wave field is characterized by waves of complex form, with lower height and lower mean period. Due to the energy transfer from the fundamental harmonic to higher harmonic components, the incident narrow-banded spectrum turns into a broad-banded spectrum (Beji and Battjes, 1993). Besides, wave interaction with LCS gives rise to a series of three-dimensional phenomena, such as diffraction, 3D wave breaking and currents system generation, that will not be studied in the present report exclusively dedicated to 2D processes.

The breaking process over the overtopped structure enhances the pumping of wave-induced mass fluxes over the low-crested detached structure. This results in an enhanced nearshore circulation and consequently the presence of the LCS modifies the sediment fluxes and morphodynamic evolution. Furthermore, the fluxes through the permeable structure may also contribute to additional modifications. Consequently circulation and morphodynamic models assessing morphodynamic evolution in the presence of LCS should include additional information regarding the fluxes on the top and through the structure.

It is well established that hydrodynamic forces due to breaking waves are among the most important sources of shore organism distribution and mortality. Therefore, in order to interpret the biomechanical characteristics of the epibiota on a low-crested structure; stress levels resulting in tissue damages or complete dislodgement; average flow conditions to predict larval settlement and delivery of nutrients or critical periods of very low flow speed causing hypoxia; a feasible description of the flow is required.

These are only possible based on an appropriate modelling of the velocity field and breaking processes in the near field of the structure and how those are affected by incident wave parameters, structure geometry and permeable material characteristics. However, it has to be pointed out that the different applications do not really require the knowledge of the turbulence fluctuations velocity components. The knowledge of the instantaneous mean flow, the seepage velocity, the maximum or minimum mean velocities is sufficient to fullfill most of the questions raised with regard to stability, functionality or ecological issues.

Therefore, an accurate description of all the above mentioned wave transformation processes is needed to correctly assess the performance of the LCS but the evaluation of the turbulence velocities is not really critical at this point.

A series of studies have led through the years to a deeper knowledge of the low porous structures near-field and far-field influence, based on theoretical, experimental and numerical investigations. The complexity of the phenomena involved in the wave field interaction with LCS has led a great majority of investigators to resort to laboratory experiments, focusing especially on the prediction of wave transmission, reflection and energy dissipation. This is the case of works by Dick and Brebner (1968), Dattatri *et al.* (1978), Seelig (1980), Davies *et al.* (1993), D'Angremond *et al.* (1996), Loveless and Debski (1997) or Seabrook and Hall (1998). Hattori and Sakai (1994) examined the conditions of incipient breaking over a permeable submerged structure. Loveless *et al.* (1998) focused on the phenomenon of sea level set-up behind detached breakwaters, previously investigated by Diskin *et al.* (1970), and pointed out the problem of water piling-up at the lee of low-crested structures in 2DV experiments.

Nonetheless, experimental investigation on low-crested structures has multifold problems: small-scale experiments are influenced by scale effects, large-scale models are expensive to build and measurements within breaking waves can be very complex, due to the aerated and transient nature of the water surface. As a consequence, alternative approaches, theoretical or numerical, have been considered for the study of wave-structure interaction. Theoretical approaches for sub-aerial breakwaters have been presented by Sollit and Cross (1972), Madsen and White (1976), Massel and Butowski (1980), Dalrymple *et al.* (1991), Losada *et al.* (1993). Wave transformation over submerged permeable breakwaters based on linear wave theory has been studied by Rojanakamthorn *et al.* (1989, 1990). Losada *et al.* (1996a, b) studied the hydrodynamics induced inside and outside a submerged permeable structure of rectangular or trapezoidal cross section under incoming regular wave trains, assuming potential flow and linear theory.

The progress in computation resources and the possibility of dealing with increasingly complex geometries has made the numerical approach more valuable. Kobayashi and Wurjanto (1989) developed a finite-difference model based on the shallow water

equations for the study of monochromatic wave reflection, breaking and transmission over a submerged breakwater, but did not take into account the permeability of the breakwater. Wibbeler and Oumeraci (1992) presented a finite element model for the simulation of the wave-induced flow in a sub-aerial porous structure. Ohyama and Nadaoka (1992) modelled the transformation of nonlinear waves passing over a submerged impermeable breakwater using the boundary element method. Gu and Wang (1992) also used a boundary element method to model the interaction of monochromatic waves with breakwaters of irregular cross section, considering dissipation due to percolation and breaking effects. The model developed by van Gent *et al.* (1994), based on the 2DV Navier-Stokes equations and the Volume Of Fluid (VOF) method introduced by Hirt and Nichols (1981), can simulate wave motions inside and outside permeable structures, including breaking conditions, but does not take into account the turbulence generation-dissipation inside the porous media. Previous works on the same model were presented by Van der Meer *et al.* (1992) and Petit *et al.* (1994a, b). Other models based on Navier-Stokes equations using the SOLA-VOF method have been presented by Iwata *et al.* (1996) to investigate wave breaking features on a submerged impermeable structure and more recently by Troch and de Rouck (1998) for the simulation of wave interaction with a rubble-mound breakwater. Lin and Liu (1998) presented a VOF-type numerical model for studying the evolution of a wave train, shoaling and breaking in the surf zone, based on the Reynolds equations with a nonlinear k-ε model. Liu *et al.* (1999) included wave interaction with porous structures. Hsu *et al.* (2002) proposed a set of equations based on the Volume-Averaged/Reynolds Averaged Navier-Stokes (VARANS) equations to describe wave interaction with coastal structures. Volume-averaging allows the description of small-scale turbulence effects in the porous media. Hur and Mizutani (2003) investigated numerically the wave forces acting on a two-dimensional body installed on a submerged porous breakwater, combining the VOF and porous body models. Three dimensional results are also presented. However, computational efforts for three dimensional models based on RANS equations as well as LES (Large Eddy Simulation) approximations are still very time consuming nowadays. To date, the models based on two-dimensional RANS approximation are possibly the most adapted to the study of wave-structure interaction for engineering purposes, as computational efforts are reasonable and the number of simplifying assumptions is considerably reduced compared to other existing models.

As a conclusion of this review, a great number of investigations have been carried out in order to characterize the performance of low-crested structures, but few of these works considered the whole set of hydrodynamic processes associated with this type of structures. The numerical approach, with a model able to simulate wave breaking processes and porous flow effects, seems the most adequate for the study of nonbreaking and breaking wave interaction with low-crested structures. The model used in the present woek is the COrnell BReaking waves And Structures (COBRAS) model, initially developed by Lin (1998). This model has been used in previous works by Lin and Liu (1998) and Lara (2002, 2003) for the modelling of wave breaking over impermeable and permeable beds, or, as mentioned earlier, by Liu *et al.* (1999, 2000) and Hsu *et al.* (2002) for wave interaction with porous structures. The model considers wave reflection, transmission, overtopping and breaking due to transient nonlinear waves including turbulence in the fluid domain and in the permeable regions for any kind of geometry and number of layers. Therefore, this model in combination with good experimental data is the best source to evaluate velocity fields around and inside LCS.

This report is organized as follows. After the introduction and review of the state of the art, the experimental information on velocities available within DELOS is presented. Section 3 covers the general information regarding the numerical model used to analyse the flow. Section 4 is devoted to the calibration and validation of the numerical model based on the experimental information presented. In section 5 and based on the numerical and experimental information, the influence on the flow of: incident wave conditions; return flow system; structure freeboard and crest width are analysed. Finally, some conclusions and comments are included.

2. Experimental information on velocities within DELOS

2.1 Experimental set–up

The experiments were carried out in the wave and current flume of the Coastal Laboratory of the University of Cantabria. The wave flume is 24.05 m long, 0.60 m wide and 0.80 m high and is divided, as can be seen in Figure 1, in different zones. The piston–type wavemaker has two attached free surface wave gauges integrated in an Active Wave Absorption System (AWACS®) that allows the absorption of reflected waves. The wavemaker and the rear absorbing beach occupy 4 m at one of the ends of the flume. The following 4 m are occupied by a false bottom that can be partially or totally removed to set off a current in the flume. The current generation system is a reversible pumping system including two zones of flow injection or sink through the bottom of the flume, two pumps, with a combined maximum discharge of 150 l/s, and a recirculation pipe. The remaining 16 m of the flume are available for the testing of models. Bottom and side walls of the testing area are made of glass, allowing the use of laser velocimetry techniques.

Two rubble-mound low-crested structures of 0.25 m and 1.00 m crest width, were tested. Crest elevation from the bottom (0.25 m), front and back slope angles (1V/2H) and rubble characteristics were maintained constant for both structures. The models had a two-layer armour of selected gravel and a gravel core. Armour and core characteristics are shown in Table 1.

	W_{15}	W_{50}	W_{85}	porosity	density
	[g]	[g]	[g]	[-]	[kg/m^3]
armour	119	153	206	0.53	2647
core	3.14	4.31	5.60	0.49	2607

Table 1. Characteristics of the gravels used for the models.

The low-crested structure model was built over a 3.8-m-long stainless steel horizontal false bottom, 0.10 m over the glass bottom of the flume, Figure 1. In the frontal foot of the rubble, a Plexiglas ramp with a 1V/20 H slope connected the false bottom with the bottom of the flume. In the rear end, another 8-m 1V/20H Plexiglas ramp simulated the

rear beach, working as an energy dissipator in order to minimize the effects on the model of the waves reflected at the end of the flume. Between the horizontal and the inclined false bottom, one rectangular aperture, 0.08 m wide, allowed the water to flow below the beach to the return piping system. When the waves piled off water behind the breakwater, the head drove the returning flow through the piping system to the false bottom in front of the wavemaker, thereby closing the circuit. In other words, the pumping system was not activated and the return flow system was only forced by gravity.

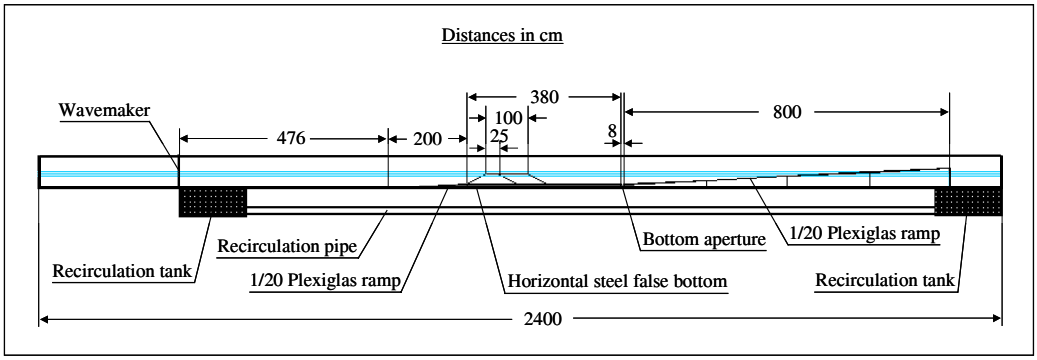

Figure 1. Definition sketch of wave flume. Experimental set-up.

2.2. Instrumentation

Among the whole set of gauges and instrumentation installed in the flume, the data used for the present study were measured by 13 resistive free surface gauges to assess free surface evolution, 3 pressure gauges inside the structure rubble and 12 Laser Doppler Velocimeter measurement points. Three free surface gauges were installed on the slope in front of the LCS to separate incident and reflected waves, Figure 2. Another two free surface gauges were located over the front slope of the structure at the same x-locations of two of the LDA measurement profiles. Two free surface gauges were placed over the structure crest and on the leeside slope. Four more were placed to measure transmitted waves along the flat bottom behind the LCS. Finally one was installed on the final beach slope. The pressure gauges, see Figure 3, were installed on the bottom, inside the LCS structure core, to measure the wave transmission inside the rubble mound.

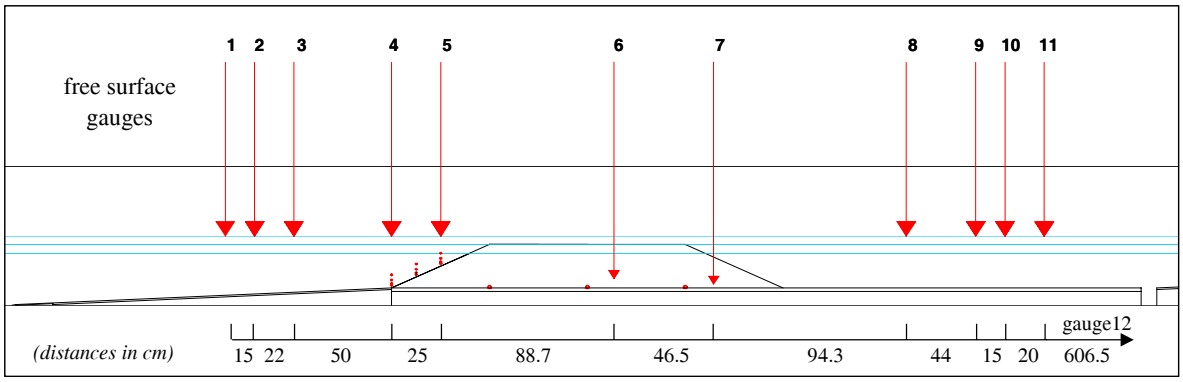

Figure 2. Instruments and measurement points around and inside the structure.

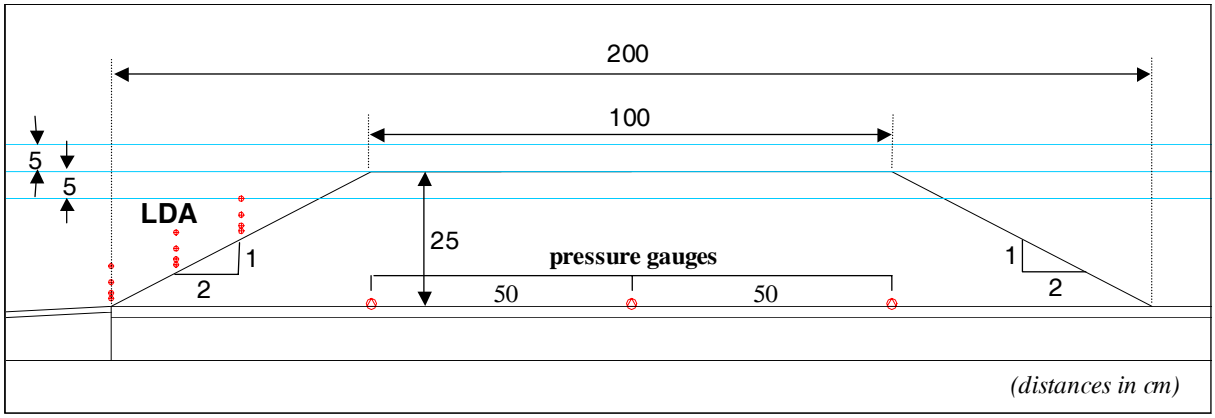

Figure 3. Close–up of the instruments over and inside the structure.

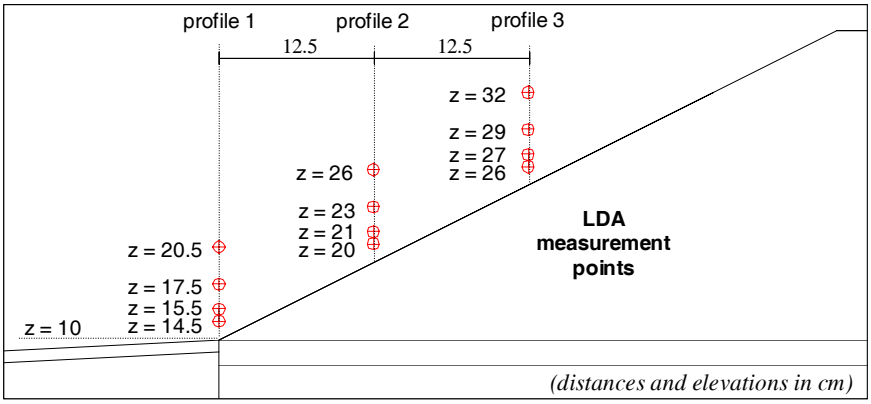

Figure 4. LDA measurement points location. Front side of the structure.

2.3. Wave tests

Two different models (0.25 and 1.00 m crest width) were tested for three different water depths (0.30, 0.35 and 0.40 m) or three different freeboards (-0.05, 0 and 0.05 m). Regular and random waves were tested. The total number of different wave conditions was 54 for both regular and irregular waves for a total of 108. The present study will focus exclusively on the interaction of regular waves with the wide-crested breakwater model. Target wave conditions are indicated in Table 2.

wave type		regular
wave height	H [m]	0.05, 0.10, 0.15
wave period	T [s]	1.6, 2.4, 3.2
water depth at wave paddle	h [m]	0.30, 0.35, 0.40
wave length at wave paddle	L [m]	2.53 to 6.17
wave steepness	H/L	0.0081 to 0.0593
relative freeboard	F/H	-1.00 to 1.00
realtive crest width	B/L	0.1621 to 0.3953
relative wave height	H/h	0.125 to 0.500
relative depth	h/L	0.0586 to 0.1580

Table 2. Target parameters for generated waves.

3. Numerical information

The information on velocities in the surface region and inside the low crested structures has been obtained based on a numerical model. The numerical model has been validated using the experimental information. Additional information has been obtained for additional geometries, permeable material characteristics and incident wave conditions. Further details on the experimental work can be found in deliverable D32 "Wave channel experimental final form".

3.1. Description of the numerical model

The present study uses the COrnell BReaking waves and Structures (COBRAS) model, whose main features are summarized in this section. The original model, named RIPPLE and developed at Los Alamos National Laboratory (Kothe *et al.*, 1991), is a general program for two-dimensional, transient, free surface incompressible fluid dynamics. It has been modified at Cornell University to deal specifically with coastal engineering issues, in particular breaking wave action and flow within porous media. Details can be found in Lin (1998), Lin and Liu (1998, 1999), Liu *et al.* (1999, 2000) and Hsu *et al.* (2002).

3.2. Mathematical formulation

The COBRAS model solves the 2DV Reynolds Averaged Navier-Stokes (RANS) equations, based on the decomposition of the instantaneous velocity and pressure fields into mean and turbulent components. Reynolds stresses are closed with an algebraic nonlinear k-ε turbulence model, that can solve anisotropic-eddy-viscosity turbulent flows. The direct resolution of the flow field inside the porous media is not practical, given the complex structure of porous materials. Consequently, the flow in the porous structure is described in the COBRAS model by the Volume-Averaged Reynolds Averaged Navier-Stokes (VARANS) equations, obtained by integration of the RANS equations in a control volume larger than the pore structure but smaller than the characteristic length scale of the flow (see Hsu *et al.*, 2002). Another set of k-ε equations similar to the previous one is used to model turbulence production-dissipation within the porous media.

3.3. Boundary and initial conditions

The boundary conditions for the mean flow field consist of a no-slip condition at the solid boundaries and a zero-stress condition at the free surface. With respect to the turbulence field, a log-law distribution of the mean tangential velocity in the turbulent boundary layer is considered near the solid boundary, where the values of k (turbulent kinetic energy) and ε (dissipation rate of turbulent kinetic energy) can be expressed as functions of the distance from the solid boundary and the mean tangential velocity outside the viscous sublayer. On the free surface, the zero gradient boundary conditions for both k and ε are based on the assumption of no turbulence exchange between the water and air. The initial condition consists of a still water situation, with no wave or current motion.

3.4. Wave generation

The COBRAS model includes a procedure of wave generation using an internal wave maker. The method consists of introducing a source function in the continuity equation for a group of cells defining the source region. The free surface above the source region responds to a pressure increment defined within the source region cells, and a train of surface gravity waves is generated. See Lin and Liu (1999) for more details. A sponge-layer method, as proposed by Israeli and Orszag (1981), is used to absorb the waves that propagate in the direction opposite the zone of interest, with an imposed exponential damping law.

3.5. Computational domain and free surface tracking method

The computational domain in the COBRAS model is discretized in rectangular cells. The computing mesh can be divided into submesh regions, which allows a variable cells spacing: a finer grid can be defined for the representation of specific study zones. The free surface is tracked using the Volume Of Fluid (VOF) method developed by Hirt and Nichols (1981) that identifies the free surface location tracking the density change in each cell. Besides, the model allows the definition of flow obstacles using a partial cell treatment. See Lin (1998) for further information.

3.6. Numerical resolution

The Reynolds equations are solved using a finite differences two-step projection method (Chorin, 1968). A complete description of the numerical resolution process can be found in Lin (1998).

4. Model calibration and validation

In this section the numerical model calibration and validation are presented and the main aspects of wave interaction with low-crested breakwaters investigated.

First the computational mesh is described and then the results of the numerical simulations are presented. The first part of the results presentation is dedicated to the model calibration, carried out with one selected test. The model validation consists then of the comparative analysis of the experimental observations with the numerical results for different wave conditions. Once validated, the numerical information is used to investigate the influence of the flow recirculation system and the structure freeboard on the flow pattern.

4.1. Mesh description

The computational mesh designed for the numerical simulation of the experiments described in section 2 is presented in Figure 5. The vertical and horizontal axes of the sketch are not scaled. As can be seen, the general configuration of the tests is reproduced, with the complete set of obstacles (slopes, false bottom) and porous media, along with the recirculation system including apertures and return flow pipe. The mesh is formed by 4 submesh regions with different grid sizes. The grid is uniform in the y-direction, but in the x-direction the cell dimension varies from 4 cm in the generation region, without high resolution requirements, to 1 cm in the vicinity of the structure which is the zone of interest. The model's ability to deal with nonuniform meshes allows considerable savings of computational time. Waves of different periods are modelled with different meshes, according to the rules of thumb for the design of the wave generation zone proposed by Lin (1998). The total number of cells is 80 in the y-direction and varies in the x-direction from 1290 for the short waves propagation up to 1749 in the case of the longest waves.

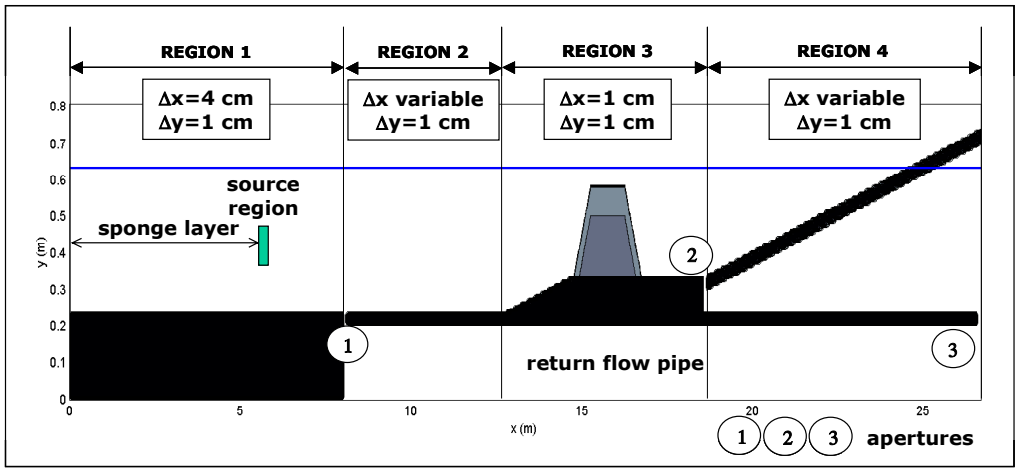

Figure 5. Sketch of the computational mesh (axes not scaled).

4.2. Model calibration/validation

The first step of the numerical simulations consists of the calibration of the model, specifically the calibration of the α and β parameters governing the flow inside the porous structure. The model calibration was carried out using a reference test with the following wave conditions: h = 40 cm, H = 7 cm, T = 1.6 s. The 40 cm water depth at the wave paddle is the maximum of the three tested in the present set of experiments. Thus, the 25-cm high structure, built on a 10-cm high false bottom, is submerged, with a negative 5 cm freeboard.

The low-crested structure modelled in the present study is not a homogeneous reef-type breakwater. It is formed of an armour and a core with different grain sizes and porosities, and thus different magnitudes of the associated frictional forces for a given flow. As a consequence, two pairs of α and β parameters, accounting for linear and nonlinear drag respectively in each of the porous layers (see Hsu *et al.*, 2002, for equations and nomenclature), are to be calibrated. A series of computations and comparisons with measurements was conducted with that objective, considering previous results from Shih (1990), van Gent (1994), van Gent *et al.* (1994), van Gent (1995) and Burchart and Andersen (1995) to estimate the range of possible values. The calibration process carried out for the present study led to the following results: α is taken to be equal to 1000 for both the armour layer and the core, and β equal to 0.8 and 1.2 respectively. The results of the model calibration are presented in the following figures.

Figure 6 shows the maximum and minimum wave height envelopes and the mean water level measured in the laboratory (dots) and calculated with the numerical model (solid lines). Numerical data result from a 10 waves phase-averaging, counted from 60 seconds of simulation to ensure stabilized flow conditions. As can be seen in this figure, the agreement between experimental and numerical data is very good. The model is able to simulate adequately the main features of the propagation of a wave train passing over a submerged breakwater. In terms of wave height envelopes, the whole pattern is accurately computed. Reflection on the rising front of the structure induces a partial standing wave system in the seaward region that the model is able to reproduce well. In the region of the structure crest, the wave height damping due to breaking and percolation inside the porous layer is correctly fitted. In the leeward region, the transmission pattern due to overtopping and flow through the structure is well reproduced, though the maximum wave height at the last gauges is slightly overpredicted. A quasi-standing wave pattern modulation of the waves amplitude can also be observed in the transmission region, as the transmitted waves interfere with the final slope back reflected waves. The wave amplitude modulation is less apparent than in the seaward zone as the energy level is much lower downwave of the obstacle.

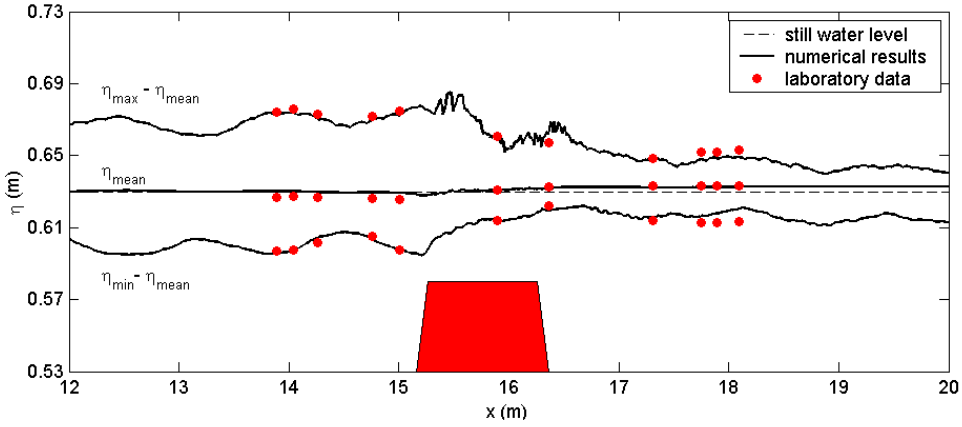

Figure 6. Wave height envelopes and mean water level.
h = 40 cm, T = 1.6 s, H = 7 cm.

The wave breaking-induced mean water level variations can be clearly observed and are well reproduced by the model: the mean water level decreases at the offshore side of the

breaking point and then increases at the onshore side. Besides, overtopping of the structure induces in the leeward zone an increase of the mean water level, of utmost importance in the dynamics of this region. As can be seen in the figure, this set-up is correctly computed.

Figure 7 displays the time series of the free surface displacement for each one of the free surface gauges presented in Figure 6, and also for gauge 12 located in the surf zone of the final beach. The solid line corresponds to the measurements and the dots to the numerical results.

The total set of free surface gauges can be divided into three groups representing the different hydrodynamic zones of the breakwater vicinity. As described in section 2, gauges 1 to 5 are located seaward of the structure, the first three on the offshore slope and the following two on the front face of the breakwater. The second zone corresponds to the structure crest, where wave breaking occurs. Free surface evolution over the crest is recorded at gauge 6. Finally time series at gauges 7 to 12 characterize the transmission zone; gauge 7 is located just on the structure leeside slope and gauge 12, as mentioned above, over the dissipative slope at the end of the flume. As can be seen, the model is able to reproduce very well the free surface time history for each one of the three regions. The incident wave train propagates on the initial gentle slope (gauges 1 to 3), then deforms and becomes more asymmetric while interfering with the rising front of the breakwater (gauges 4 and 5) until reaching an unstable situation. Then the relative crest width (crest width divided by wave length) is large enough to make the waves break over it (gauges 6 and 7). As can be seen, the use of the Volume Of Fluid technique enables the COBRAS model to reproduce with accuracy the free surface during and after wave breaking, where other numerical models for breaking waves fail to calculate the free surface. Furthermore, the VOF technique combined with RANS equations does not require the introduction of a specific breaking criterion to target wave breaking.

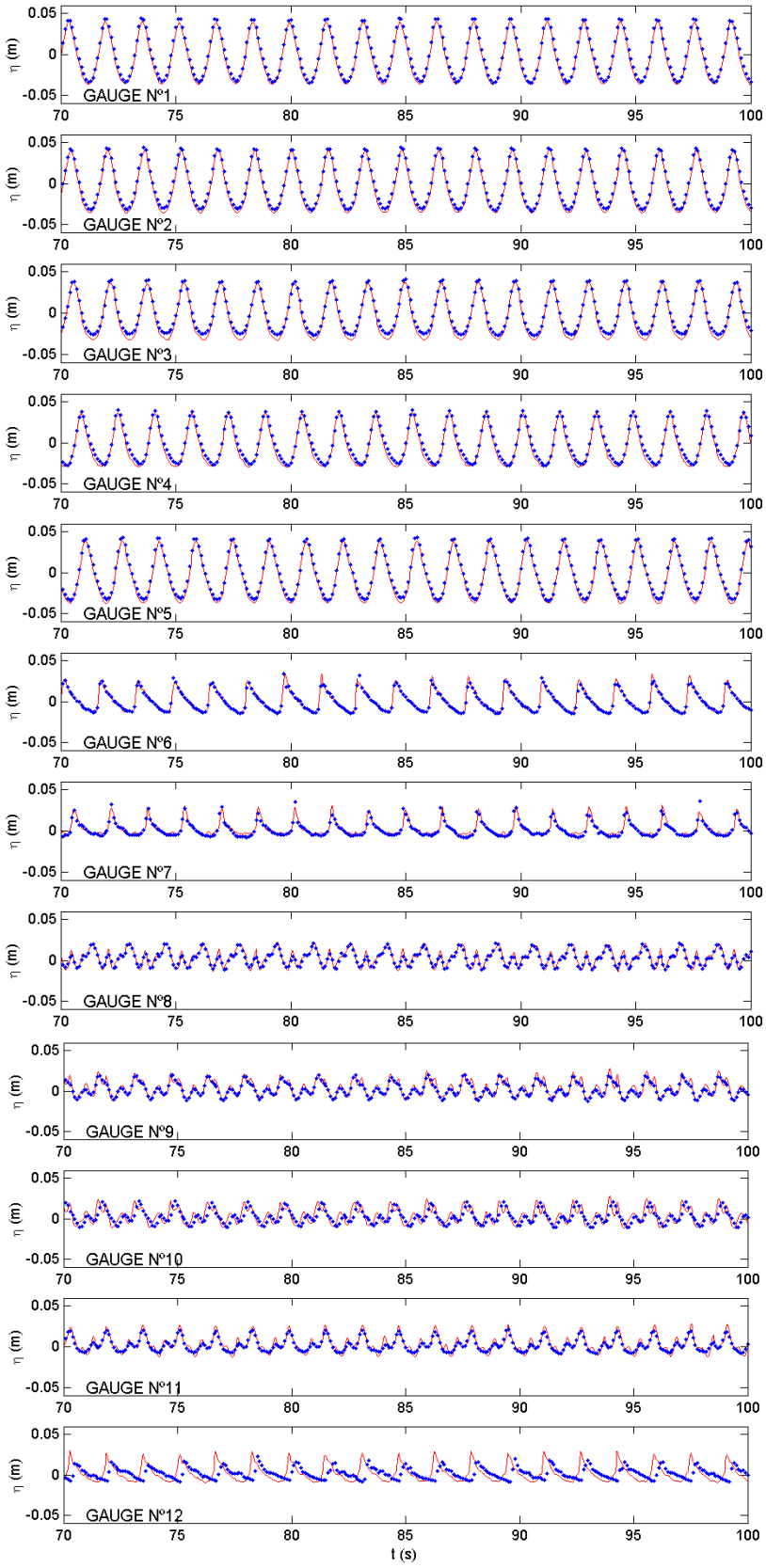

Figure 7. Free surface time series, gauges 1 to 12.

h = 40 cm, T = 1.6 s, H = 7 cm. Solid lines: experimental data. Dots: numerical results.

Wave records in the transmission zone (gauges 8 to 11) show a complex profile that the numerical model reproduces adequately. This complex wave shape, with multiple crests, accounts for the higher harmonics generation over the submerged breakwater. Nonlinear phenomena of wave-structure interaction result in the amplification of bound waves (phase-locked with the first harmonic) that are released when breaking occurs over the structure crest. In the deeper waters leeward of the obstacle, the phenomenon known as wave decomposition takes place as the free waves propagate at a different celerity than the primary wave. This phenomenon has been observed in many experimental and numerical studies like Beji and Battjes (1993) and Beji and Battjes (1994), or in field experiments by Masselink (1998) or Sénéchal *et al.* (2002), and for waves propagating over a porous step by Losada *et al.* (1997).

The energy transfer from the fundamental harmonic to higher frequencies is illustrated in Figure 8. The amplitude of the first five harmonics at each one of the gauge stations is represented for both numerical and experimental cases. The model reproduces the laboratory data with a good level of agreement. The maximum error on the first two harmonic amplitudes is 10% at station 7 and 14% at station 5 repectively. The rate of error is greater for the higher frequency components, but the corresponding amplitudes are too small (one or two orders of magnitude with respect to the first harmonic at the first six stations) for the error to be significant. At station 6, the first harmonic amplitude abruptly decreases as breaking occurs over the structure crest, coinciding with an enhancement of higher harmonics amplitude. Previously, at station 5, the fundamental harmonic amplitude increases as a result of the shoaling effect on the front side of the structure.

Once the model is calibrated in terms of free surface displacement, the numerical data are directly compared with the dynamic pressure measured inside the porous structure. The comparison between measured and computed time series of the pressure at the three stations located inside the structure, at the interface with the steel false bottom (see Figure 3), is presented in Figure 9. As can be seen, the computed pressure time series agree favourably with the corresponding measurements. The same behaviour as free surface in terms of wave attenuation can be observed: the instantaneous pressure decreases along the structure, from the exposed front slope of the breakwater to the leeside slope.

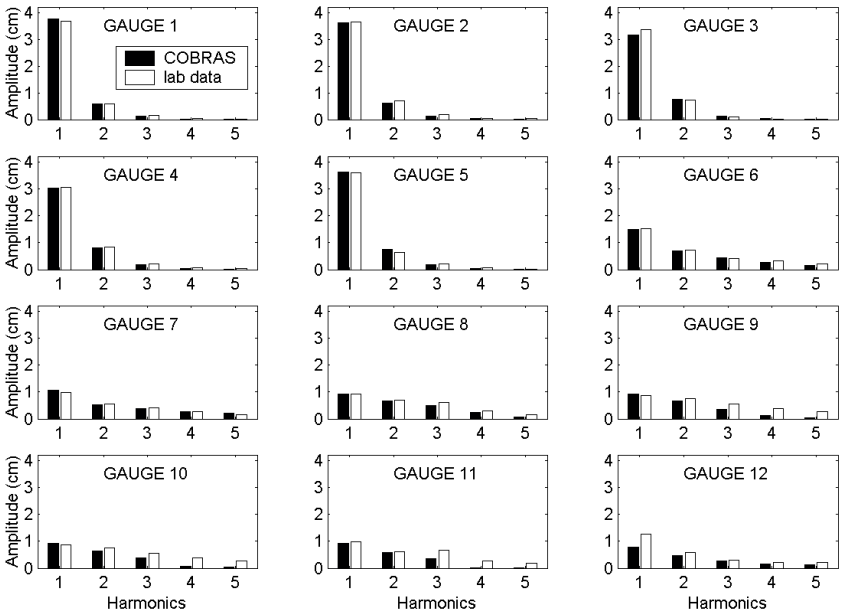

Figure 8. Harmonics amplitude, gauges 1 to 12.

h = 40 cm, T = 1.6 s, H = 7 cm.

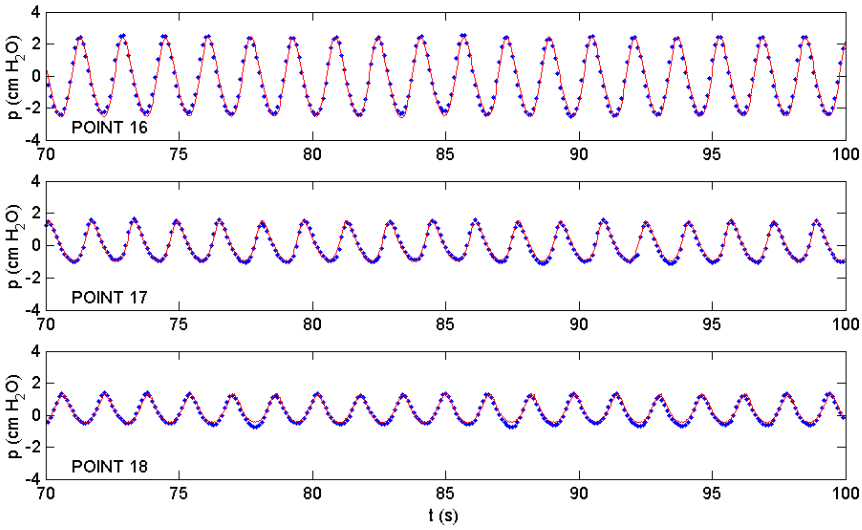

Figure 9. Pressure time series.

h = 40 cm, T = 1.6 s, H = 7 cm.

Solid lines: experimental data, dots: numerical results.

In addition to free surface displacement and pore pressure, particle velocities at the seaward slope of the structure were considered in the calibration process. The

estimation of the velocity field in the vicinity of the breakwater is of utmost importance, for instance, as a first step in the analysis of the stability of the structure. Figure 10 shows, for each one of the three profiles of measurements presented in Figure 4, the phase-averaged horizontal and vertical velocities vs. time normalized with the wave period. The first and second lines of the graphs correspond to horizontal and vertical velocities respectively, while the four columns correspond to the different elevations of measurement points. Solid and dashed lines represent experimental and numerical data respectively. As can be seen, the agreement is rather good, in terms of amplitude and wave profile. The highest discrepancies appear at profile 1, at the point nearest to the structure bottom (z = 14.5 cm), where local effects of the stones is the most likely to perturb the measurement. It has to be pointed out that obstacles in the computational domain are defined through a partial cell treatment allowing the obstacles slopes to intersect the cells and not to be saw tooth-shaped. As a result, the numerical model deals with a smooth-faced breakwater while measurements in the laboratory are taken on a rubble-faced structure.

The tests simulated with the same water depth (h = 40 cm) but with different wave heights and periods show no great influence of these variables on the model performance. The coefficients α and β are kept constant and are not used as adjusting parameters for each of the different tests. Figure 11 shows the results of wave height envelopes and mean water level for different wave conditions. Figure 11a and 11b correspond to higher (10 cm wave height) and smaller (3.6 cm) waves respectively than in the previous case (7 cm), with the same period (1.6 s). Influence of the wave period can be appreciated by comparing Figures 11b to 11d, corresponding to 1.6, 2.4 and 3.2 s wave periods respectively for the same wave height. For all these cases the wave field around the submerged breakwater is well reproduced by the numerical model. In the case of the largest incident waves, the discrepancies between experimental and numerical data are more pronounced, especially for the maximum wave height envelope which is quite overestimated seaward of the structure. This is due to the fact that the selected values for α and β are not optima for the high Reynolds number flow conditions induced by this extreme value of wave height, about three times the wave height of cases (b) to (d). The small discrepancies in the transmission zone observed in the simulation of the shortest waves (Figures 6, 11a and 11b) are reduced when wave period is increased. Wave breaking is clearly different compared to the previous case,

turning from plunging for high and intermediate waves to spilling in the case of the smallest waves. An increase in wave period moves the breaking point in the onshore direction. The short waves break over the very beginning of the crest zone, while breaking of the longer waves occur at the landward limit of the crest zone.

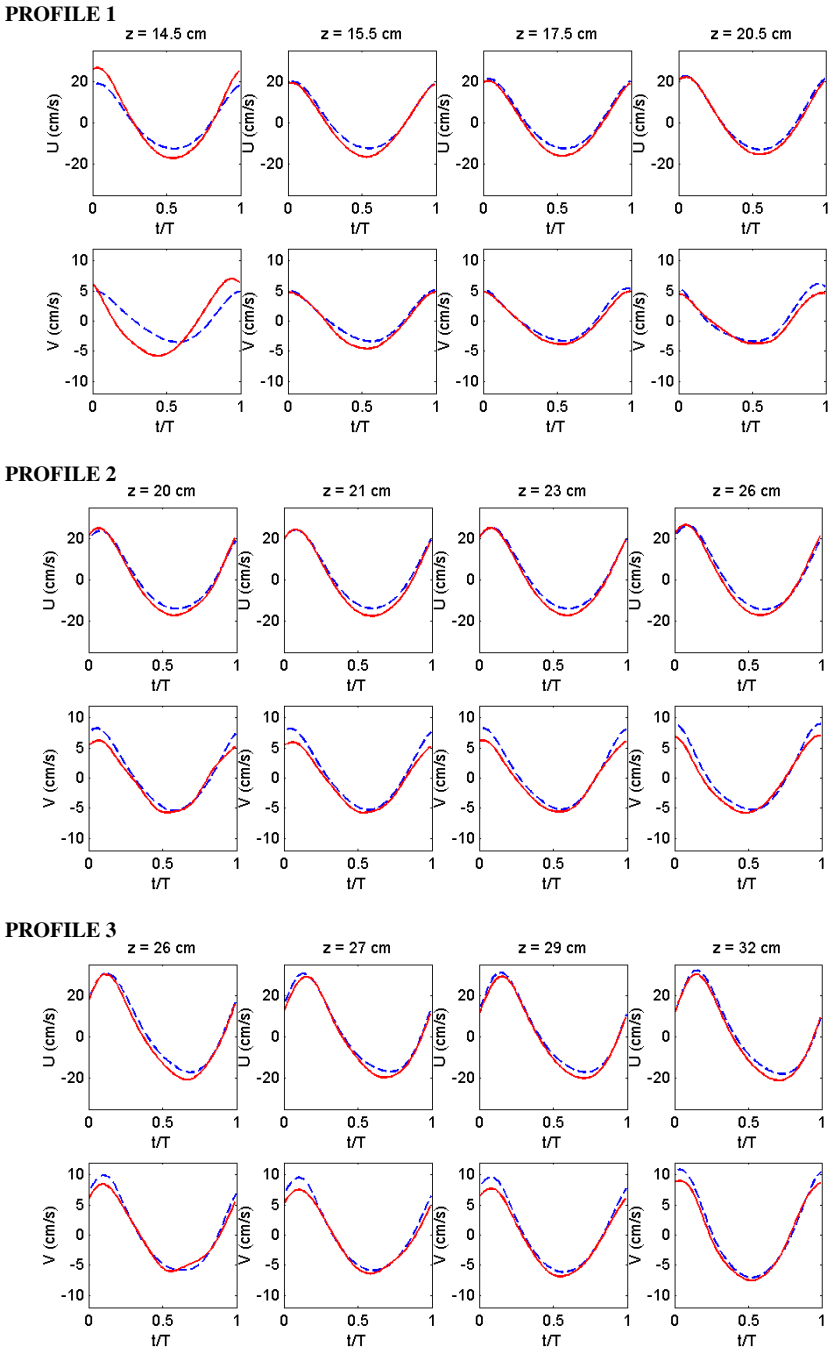

Figure 10. Phase-averaged velocities.

h = 40 cm, T = 1.6 s, H = 7 cm.

Solid lines: experimental dat. Dashed lines: numerical results.

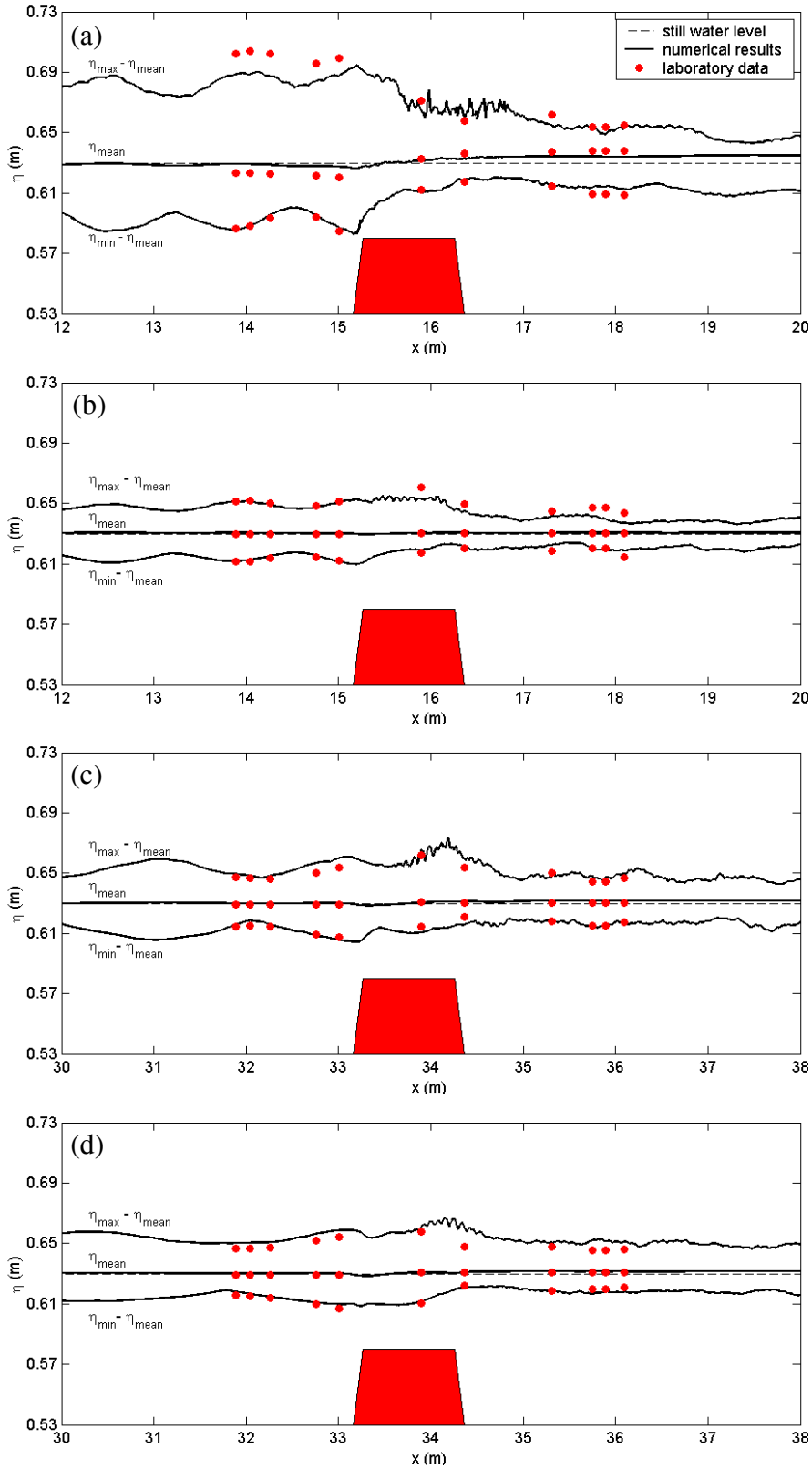

Figure 11. Wave height envelopes and mean water level.

(a) h = 40 cm, T = 1.6 s, H = 10 cm.(b) h = 40 cm, T = 1.6 s, H = 3.7 cm. (c) h = 40 cm, T = 2.4 s, H = 3.7 cm.(d) h = 40 cm, T = 3.2 s, H = 3.7 cm.

As a first conclusion, the model is proven to simulate the hydrodynamic behaviour of a submerged structure with a high degree of agreement with experimental observations. The values of the porous media parameters set for the simulation of H = 7 cm, T = 1.6 s waves, are validated and are proven to give satisfying results independently of the wave height and period. It is important to point out that the results presented in Figure 11 can be improved and the commented discrepancies removed by adjusting the porous media parameters depending on the wave conditions. Nonetheless, the objective of the present calibration is to fit the breakwater response using constant values of these porous media parameters for any conditions of flow, in order to show the model's ability as a predictive tool.

Therefore, in contrast with previously existing models for wave interaction with permeable low-crested structures, it can be said that the model performs reasonably well for all the magnitudes considered, i.e. wave envelopes, free surface evolution, velocities and pressure and for different incident wave conditions.

5. Analysis of results

5.1. Introduction

In this section, three additional tests are presented and compared with the reference test (h = 40 cm, H = 7 cm, T = 1.6 s) included in the previous section. The corresponding numerical simulations are mainly used to investigate two important aspects. First, the influence of the recirculation system described in section 2 on the near-structure flow conditions is studied. Next, the influence of the freeboard is considered and results of wave interaction with zero and positive freeboard structures are presented. Finally, the influence of the cres width will be analyse. These aspects are studied based on a combination of experimental and numerical results. As it will be shown, one of the main advantages of the model is the possibility of numerically reproducing several magnitudes that either cannot be measured or require an intensive and expensive experimental programme.

5.2. Influence of the return flow system

Low-crested structures are by definition strongly overtopped structures, designed to allow the transmission of a certain amount of the incident wave energy. In most 2-D laboratory experiments on this type of structures, the overtopping gives rise to a piling-up of water in the leeside region of the structure and hence to an increase of the mean water level pointed out, for instance, by Loveless and Debski (1997). This set-up in the transmission zone modifies the dynamics of the waves reformed in this region and the flow conditions in the vicinity of the breakwater. It forces a strong return flow over the structure which perturbs the wave breaking process on the structure seaward slope and crest, influencing the breaker type, position and height. In real cases of stretches of shore protected by low-crested structures, this phenomenon is not observed, as the potential piling-up behind the breakwater is relieved by 3-D circulation systems. Part of the flow is transmitted back to the seaward side through the permeable structure, but a greater proportion returns to the open sea by the sides of the breakwater, following pathways of lesser resistance. The configuration of the laboratory tests conducted for

this study has been thought to prevent this usual shortcoming of 2-D experiments consisting of a non-realistic set-up leeward of the low-crested breakwater.

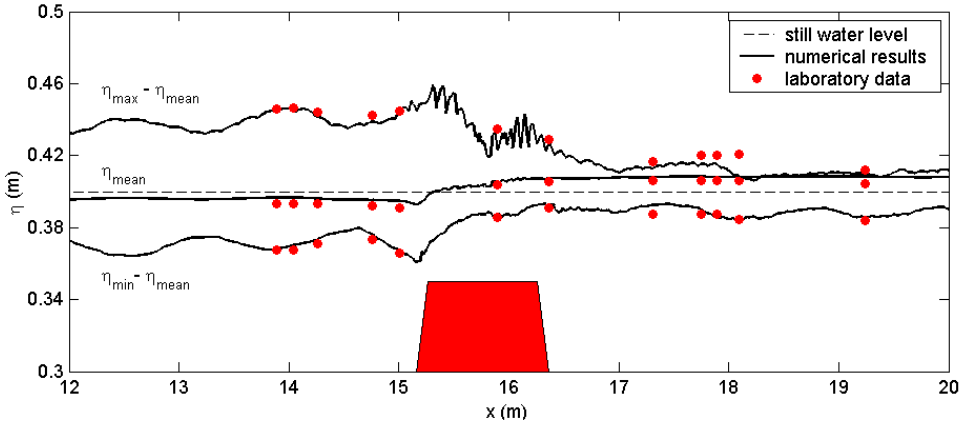

Figure 12. Wave height envelopes and mean water level.
h = 40 cm, T = 1.6 s, H = 7 cm. No flow recirculation.

To examine the influence of the flow recirculation system described in section 2, a laboratory test without recirculation was conducted, with the same wave conditions as the reference test. Thus the structure considered in this test is submerged, with a negative 5 cm freeboard. Figure 12 shows the results of surface elevation envelopes and mean water level when no flow recirculation is considered. The same high degree of agreement between experimental and numerical data is obtained as for the equivalent test including flow recirculation. The wave height patterns at both sides of the structure are well tracked: the model adequately reproduces the breakwater performance in terms of reflection and transmission. The set-down previous to wave breaking above the seaside slope of the structure and the post-breaking set-up in the leeward zone are adequately simulated. The excessive value of the set-up in the transmission region due to overtopping as commented earlier is correctly predicted.

It can be seen that the mean water level in the leaward zone is significantly higher in the case where recirculation is not allowed compared to the reference test. Wave height envelopes in the transmission zone, as well as wave breaking over the structure crest, are also influenced by the flow recirculation system. Thus, comparing Figures 6 and 12, it can be concluded that the flow recirculation system is checked to work properly, in both the experimental and numerical wave flumes.

Figure 13 clearly demonstrates the influence of the flow recirculation system on the flow structure. The computed mean (ensemble-averaged) flow around and inside the breakwater is plotted, in terms of stream lines and velocity field, for both configurations, without and with recirculation. Mean flow is obtained by averaging over 5 waves starting from instant t = 60 s of the simulation.

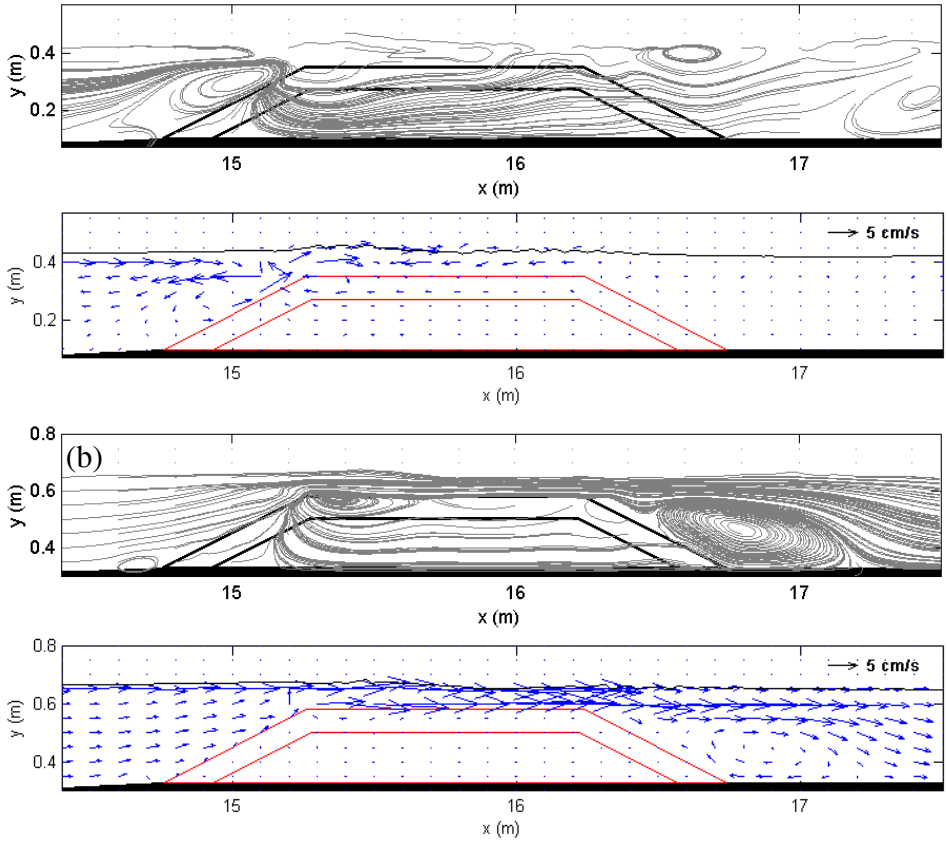

Figure 13. Computed mean (ensemble averaged) velocities:
(a) case without flow recirculation, (b) case with flow recirculation.

The mean water level increase in the transmission zone due to overtopping induces a hydraulic gradient and therefore a return flow directed offshore. In the first case where the recirculation pipe is locked, this return flow hinders the onshore transport associated with wave nonlinearity and wave breaking and gives rise to a mean current directed offshore. In the transmission zone, velocities are very low and this mean current can hardly be appreciated. Higher velocities are observed over the crest, where the reduction of the water depth induces an acceleration of the flow, and result in the formation of a vortex cell at the seaward slope of the structure.

In the case of the test including flow recirculation, the excess of water in the leeward zone due to overtopping flows back through the return pipe. This configuration allows mean motions to become well-established and to have a nature-like pattern. The overall transport is directed onshore, and the strong current over the structure crest due to flow constriction and breaking and flow separation at the crest edge originates the formation of a vortex at the leeside slope. This vortex influences the stability of the structure as the local offshore velocities at the leeside toe are responsible for the well-known scour phenomenon. Another vortex cell of smaller dimensions can be observed at the toe of the seaward slope, with the subsequent consequences on slope stability.

The vertical distribution of the mean flow, Figure 14, illustrates the significant differences between the no-recirculation and the recirculation configurations. Six sections at the breakwater vicinity have been selected and the ensemble-averaged horizontal velocity profiles at these sections have been plotted for both configurations. In the case of no recirculation, the mean current below the trough level is directed seaward, outside and inside the structure. The seaward mean velocities in the transmission zone, as can be observed at section 12 profile, are found to be very low, with a maximum value of 0.5 cm/s just below the trough level. At section 6 the vortex cell that forms at the seaward slope results in an inversion of the mean flow and an onshore near-bed component. The breaking process at the seaward edge of the structure crest allows a greater penetration of the flow and higher mean velocities inside the porous medium in this zone, as seen at the section 7 profile.

When recirculation is allowed, Figure 14b, the net transport is clearly shoreward. As mean motions are of greater intensity in that case, the horizontal scale has been reduced for reasons of clarity. At section 6 the profile under the trough level is almost uniform vertically but shows a peak value known as the overshooting effect near the structure. This phenomenon, observed by Lomonaco *et al.* (2002), consists of an acceleration of the flow, as a result of the reduction of water depth, slightly before the wave crest passes. This local velocity enhancement at the interface with the structure is obviously of great relevance regarding stone stability. Over the structure crest, mean velocities are substantially higher, as a result of flow constriction and wave breaking. Inside the porous structures, these velocities are nearly zero, or slightly negative as a consequence of the vortex cell formed leeward. The two equivalent sections in the transmission zone

show significant differences: the low negative values in the no-recirculation case become positive and about 6 times higher in the configuration with flow recirculation.

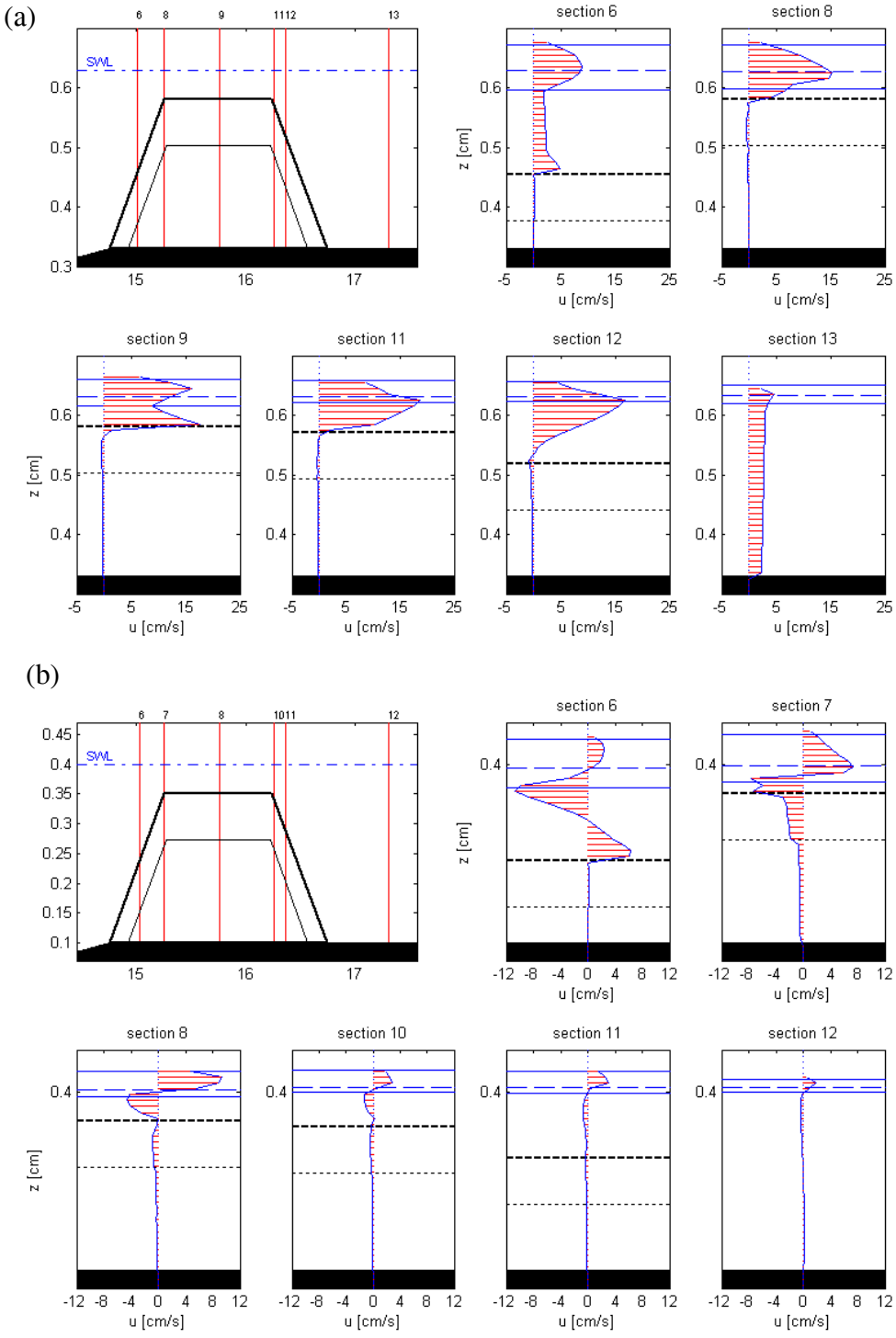

Figure 14. Computed mean (ensemble averaged) velocities:
(a) case without flow recirculation, (b) case with flow recirculation.

As a conclusion, the absence of a flow recirculation system aimed at discharging the overtopping-induced excess of mass leeward of the structure is confirmed to strongly influence the flow pattern in the flume. The flow recirculation system is found to be fundamental in the adequate 2DV modelling of the low-crested structure hydrodynamics. Besides, the COBRAS model is found to be able to deal with the complex laboratory test configuration including the flow recirculation system.

5.3. Influence of the structure freeboard

In this section a similar analysis is carried out to study the influence of the breakwater freeboard F on the flow pattern. As emphasized by d'Angremond *et al.* (1996), crest elevation relative to still water level is a crucial parameter in wave transmission, along with wave characteristics (height, period, relative depth) and the breakwater type (permeability, surface roughness). In order to analyse the influence of the structure freeboard two additional cases have been considered, with zero and positive freeboards. Flow recirculation is allowed in both cases. These two cases can be regarded as extreme cases since most of the existing models for wave and submerged or low-crested structure interaction fail to reproduce the flow field under these conditions. However, it has to be pointed out that in meso and macrotidal environments these are two cases to be considered in the design of low-crested structures.

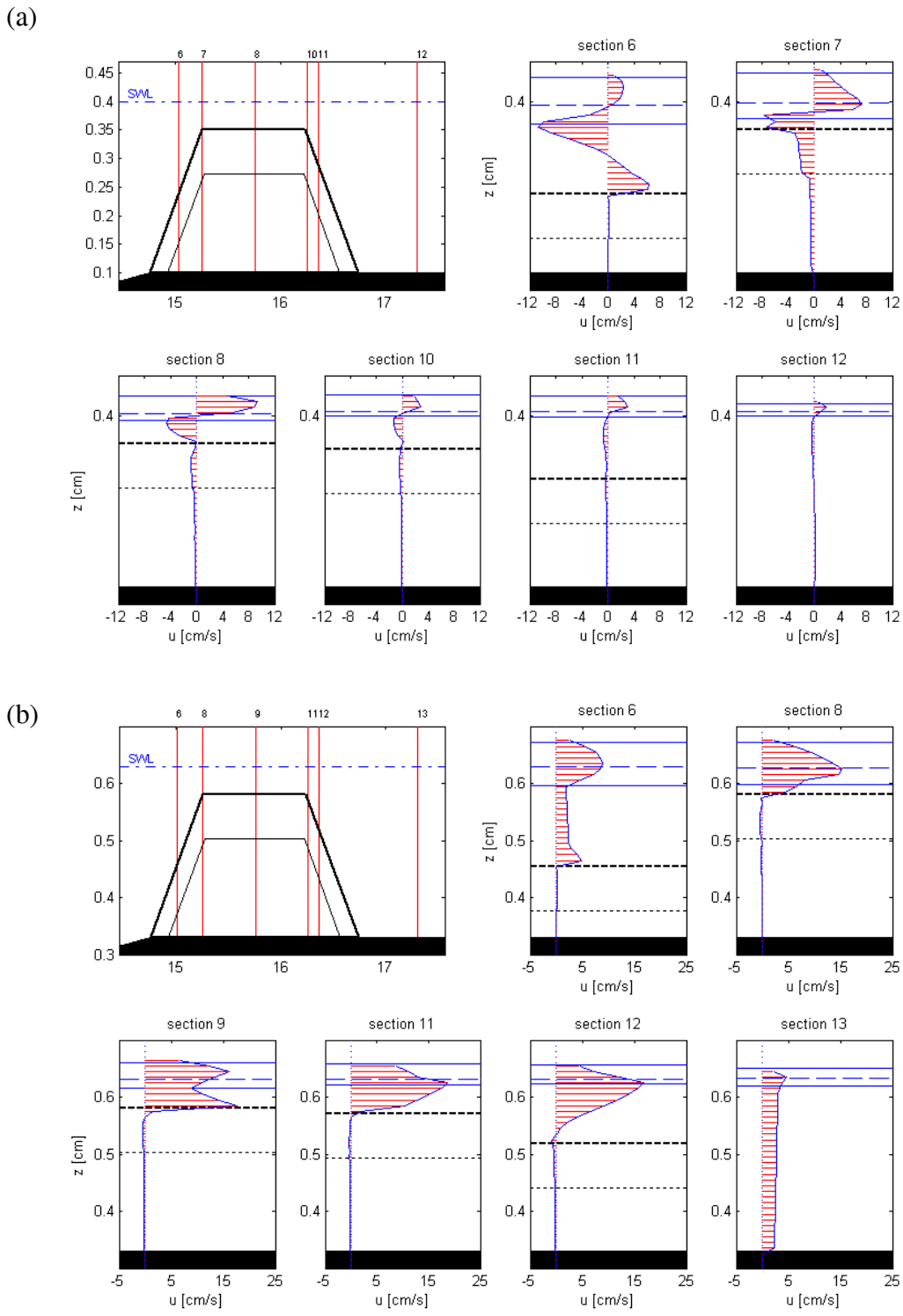

Figure 15. Computed mean (ensemble averaged) velocity profiles: (a) case without flow recirculation, (b) case with flow recirculation.

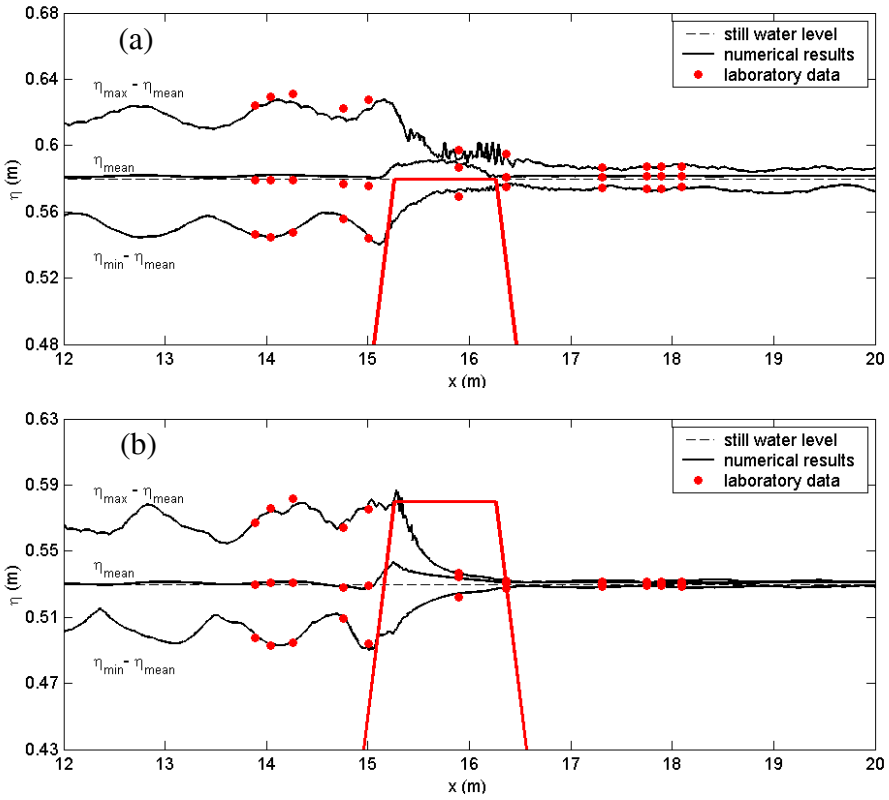

Figure 16. Wave height envelopes and mean water level.
(a) h = 35 cm, T = 1.6 s, H = 7 cm.
(b) h = 30 cm, T = 1.6 s, H = 7 cm.

As can be seen, the same high degree of agreement between experimental and numerical data as for the 40-cm water depth test is obtained. The wave envelope patterns and mean levels at both sides of the structure are well tracked: the model adequately reproduces the breakwater performance in terms of reflection and transmission.

Reflection on the structure seaward slope induces a clear partial standing wave pattern, well reproduced by the model. The same phenomenon takes place leeward of the structure, as the final beach-reflected wave combines with the breakwater-transmitted wave. In the case of the emerged breakwater, the transmitted wave height is too small for this feature to be clearly observed. For the tested wave conditions (H = 7 cm, T = 1.6 s), the zero freeboard breakwater is slightly overtopped and waves break on the seaward edge of the crest. In the case of the 5 cm freeboard structure, no overtopping occurs; waves break on the upper part of the seaward slope. Transmission only occurs through the porous structure, giving rise to a very low-perturbed landward wave field. In both

situations the set-down previous to breaking above the seaside slope of the structure and the post-breaking set-up are correctly simulated.

As pointed out by Burchart and Andersen (1995), the porous media α and β parameters are flow dependent. Still, in the previous model calibration/validation section, they were kept constant for any wave conditions in order to check the model ability to reproduce the hydrodynamics of the submerged structure. Nonetheless, flow conditions at emerged breakwaters are very different, as will be verified afterwards, and the core nonlinear drag β parameter needs to be adjusted compared with the F≤0 structure. β equal to 0.4 (instead of 1.2 for negative or null freeboard structures) was found to better fit the laboratory observations.

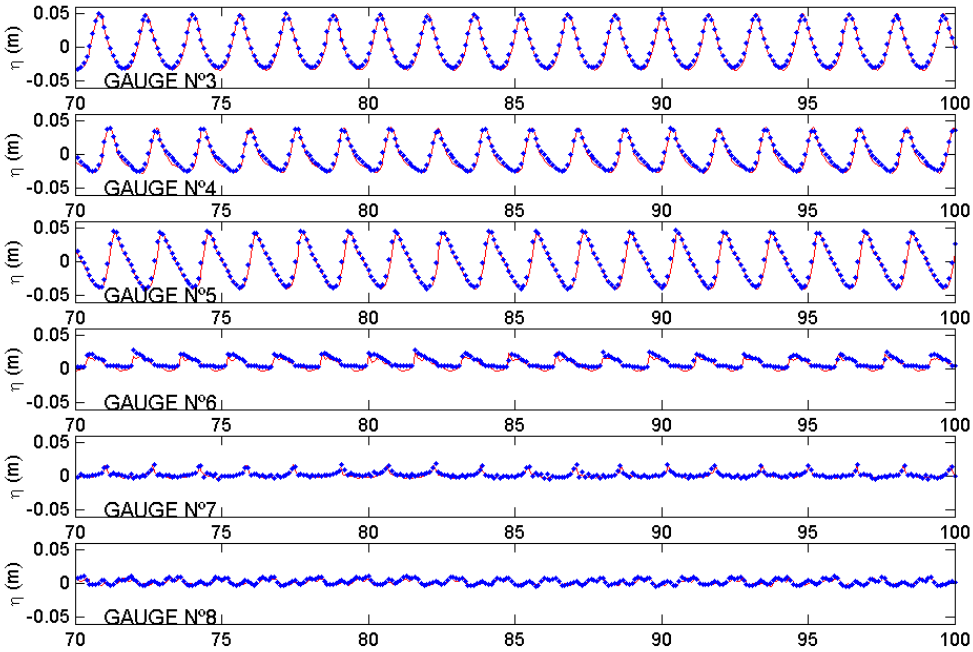

Figure 17. Free surface time series.

h = 35 cm, T = 1.6 s, H = 7 cm.

Solid lines: experimental data. Dots: numerical results.

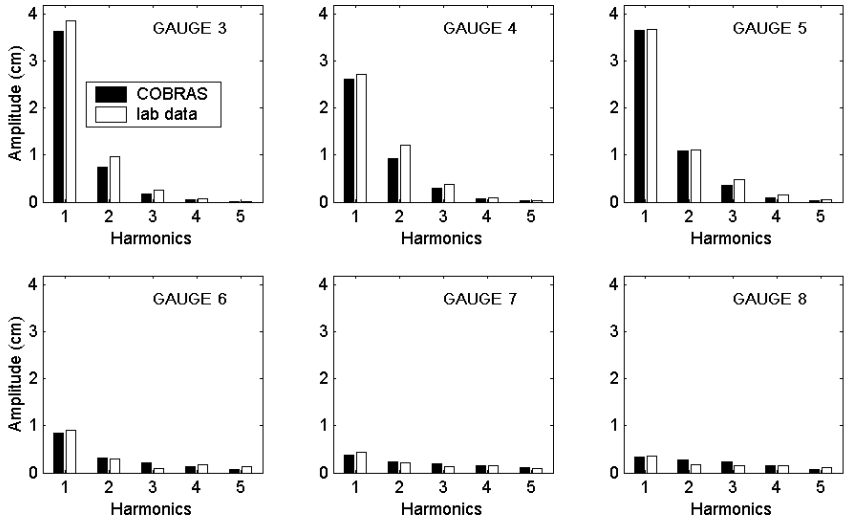

Figure 18. Harmonics amplitude, gauges 3 to 8.
h = 35 cm, T = 1.6 s, H = 7 cm.

The good performance of the model regarding the zero freeboard structure is illustrated in Figures 16 and 17. Figure 16 displays the time series of free surface displacement at gauges 3 to 8, all located in the vicinity of the structure (see Figure 2). The solid line corresponds to the measurements and the dots to the numerical results. All graphs are plotted with the same vertical scale to better visualize the substantial reduction of the wave height. The initial phases of the incident wave train evolution and transformation are the same as for the submerged breakwater: the waves get steeper while passing on the initial gentle slope and then shoals on the seaside slope of the structure. The waves adopt an unstable profile earlier, as the relative depth is smaller, and the breaking point is slightly moved seaward. As the structure crown is higher, the amount of water that overtops it is reduced and the onshore wave field is, therefore, less perturbed. It is interesting to note the model ability to deal with the specific situation of a thin film of water covering the crest of the structure (station 6). Multiple crests in the onshore wave field can be observed: also in the case of the zero freeboard breakwater the model is found to simulate adequately the nonlinear wave decomposition process.

The reduction of wave height and harmonics enhancement can be observed in Figure 18. Vertical scale is kept constant for all the gauges for an easier comparison. The model calculates the harmonics amplitudes with a reasonably good agreement. From gauge 6, located over the structure crest, wave energy is distributed over a broader range

of harmonics. The amplitude of the fundamental harmonic of the incident wave spectrum decreases considerably, as part of the incident energy is dissipated and another part redistributed to higher frequencies. At station 3 the calculated amplitude of the first harmonic is 96% of its value at station 1. It then decays to 22% in the crest zone (station 6) and to 9% leeward of the structure (station 8). The error on the first harmonic amplitude is less than 6%, except at gauge 7 where the calculated amplitude differs out of 14% from the measured one. However, the error is not very significant as the harmonic amplitude is about 4 mm at this station.

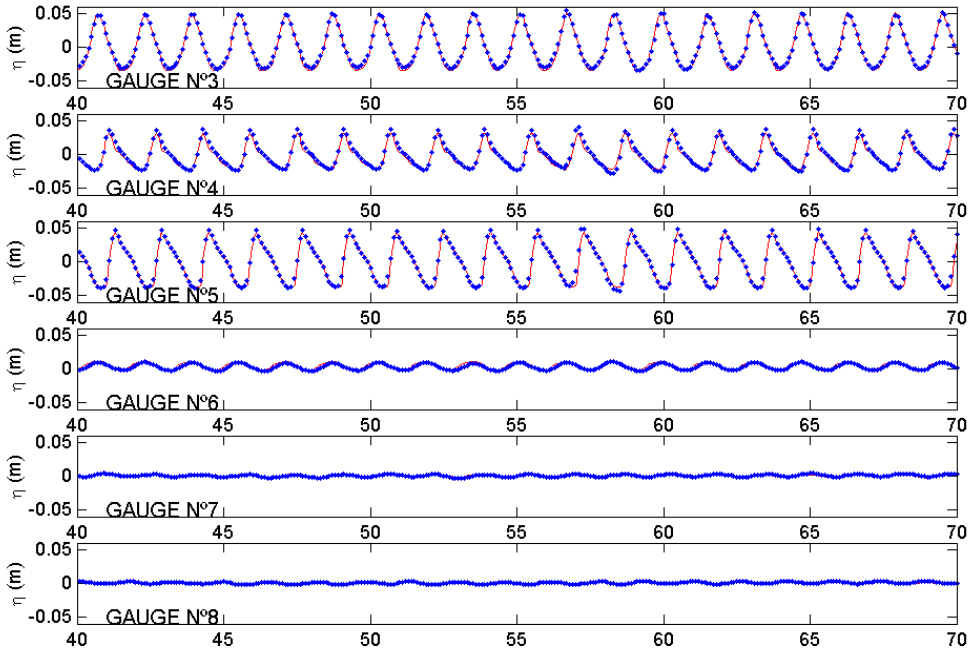

Figure 19. Free surface time series.
h = 30 cm, T = 1.6 s, H = 7 cm.
Solid lines: experimental data. Dots: numerical results.

Figures 18 and 19 correspond to the case of the +5 cm freeboard. As can be seen, the water surface displacement around and inside the emerged breakwater is well reproduced by the model. The same phenomena of wave shoaling and breaking as in the previous cases can be observed, with a slight translation seaward. Wave profile reaches an unstable shape earlier, and breaking occurs between stations 5 and 6, on the upper part of the seaward slope. Surface variations at stations 6 and 7 are recorded inside the porous structure, in the crest and leeward slope regions respectively. As can be observed, wave energy is considerably damped. The drastic reduction of the incident

wave height is clearly illustrated by Figure 20. At station 3, the calculated amplitude of the first harmonic represents 107% of its value at station 1. This percentage decreases to 17% at station 6 and 5% at station 8. The error between numerical and experimental values is about 10%, except at gauge 8 (32%) but the wave height is lower than 2 mm at this station.

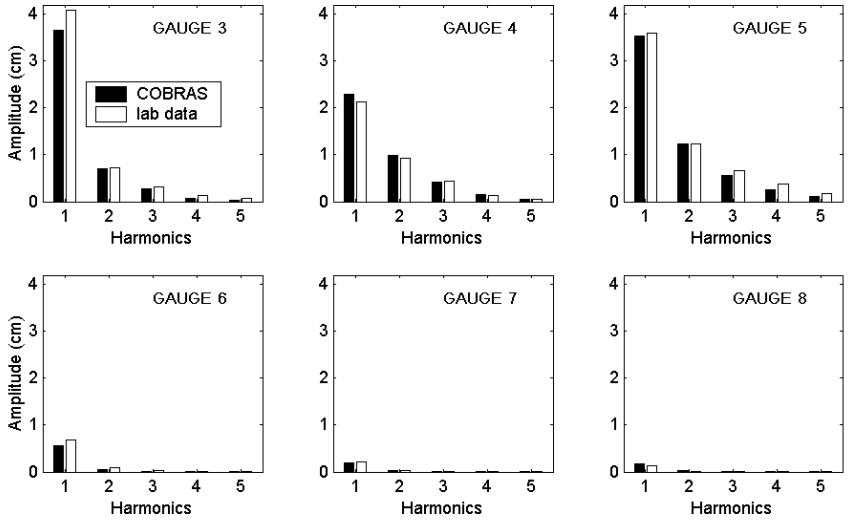

Figure 20. Harmonics amplitude, gauges 3 to 8.
h = 30 cm, T = 1.6 s, H = 7 cm.

From the results presented in Figures 15 to 19, it can be concluded that the model performance is not affected by strong variations of the freeboard. The model is able to simulate the wave interaction with a porous breakwater, whether submerged or emerged, with the same level of accuracy, despite their very different hydrodynamic behaviours. These differences are clearly illustrated by Figure 21. Snapshots of the velocity field around the structure at 4 different instants are plotted for the three tested freeboards. Wave breaking conditions are obviously affected by the structure freeboard. Spilling breakers over the crest when the structure is submerged turn into plunging on the crest seaward edge in the case of the zero freeboard, and collapsing on the seaward slope when the structure emerges. Among the three tested crest elevations, the breaking-induced peak velocities are minimum when the structure is submerged and maximum when the freeboard is zero. The seaward edge of the crest seems then to be the most vulnerable zone of the structure. When the structure is submerged, the peak velocities associated with the propagation of the roller are distributed all along the crest zone and also affect the upper part of the leeward slope.

It is important to outline the model ability to simulate the flow motions over the crest when the crown elevation coincides with the still water level. Note that the seaward edge of the crest remains alternatively submerged (t/T=0) and emerged.

In the case of the F>0 structure, as commented earlier, incident waves break over the front side slope and no overtopping occurs. As the tested structure is a rubble mound, the up-rushing wave tongue that would form over the crest if the breakwater were impermeable is transmitted into the porous media and there is finally no volume of water overtopping into the leeside water body. The portion of incident wave energy that is transmitted by the emerged rubble-mound breakwater corresponds exclusively to flow through the porous media and is thus very low. The dominant mode of energy dissipation in this case is the resistance to the flow inside the porous medium. The propagation of the dissipated wave can be clearly observed in the crest armour layer at t/T=0.7. The oscillation is totally damped at t/T=0.

The model is then found to provide valuable information on the near-structure flow conditions. This is also true in terms of mean flow, as illustrated by Figures 21 and 22. The perturbation of the mean flow pattern associated with wave breaking clearly appears in these figures. The high velocities over the crest in the case of the F = 0 structure, as commented above, give rise to a strong mean current over the structure crest and a vortex cell at the lee, as for the submerged structure. It is interesting to note the vertical symmetry of the stream lines pattern inside the structure. A smaller vortex cell forms at the seaward edge of the crest and confirms the vulnerability of this zone when F=0. Finally, a vortex cell of reduced dimensions appears at the seaward toe of the structure and may be responsible for scour phenomenon.

(a) t/T=0

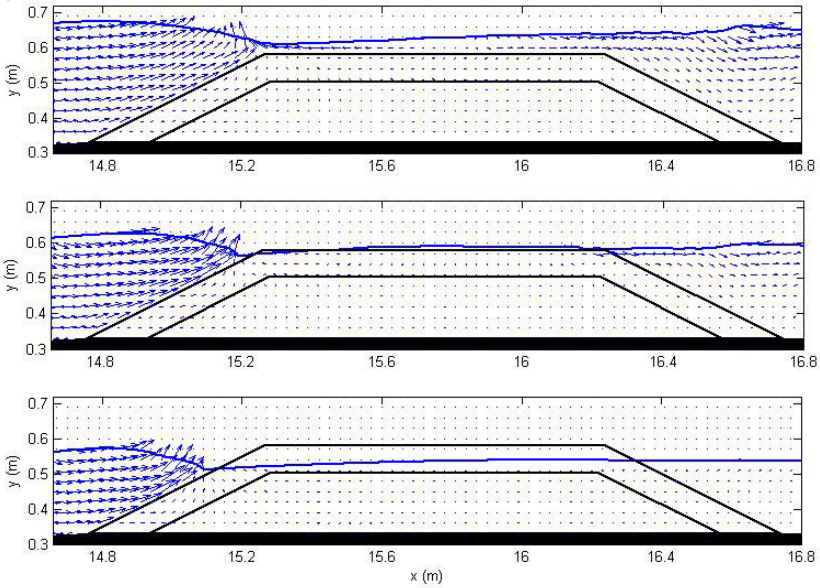

(b) t/T=0.2

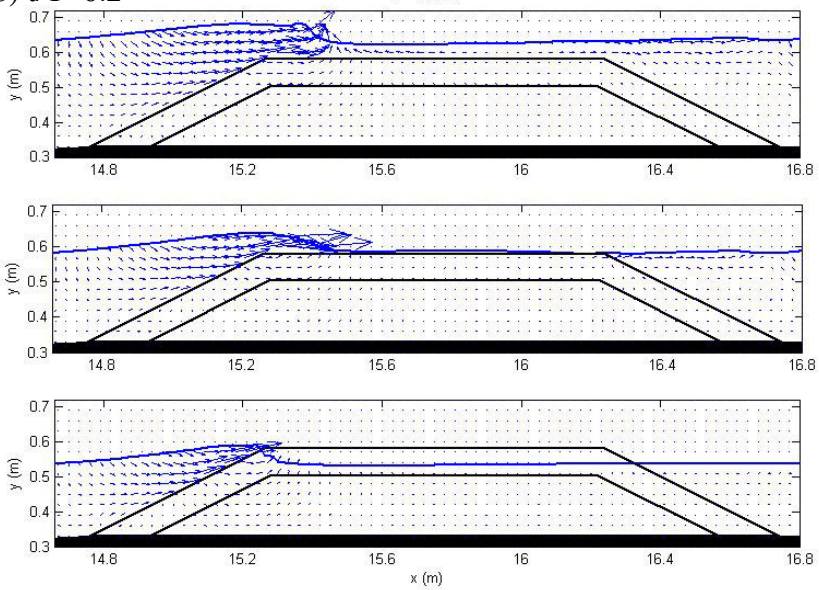

(c) t/T=0.5

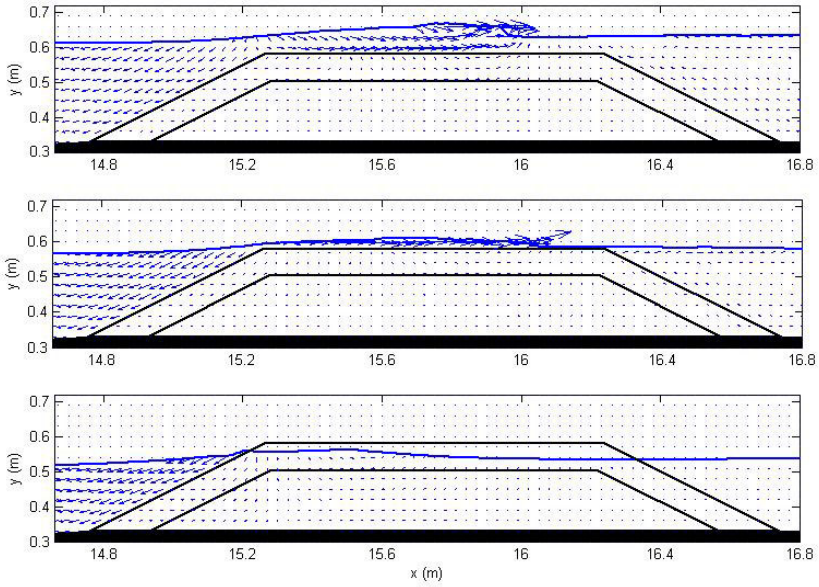

(d) t/T=0.6

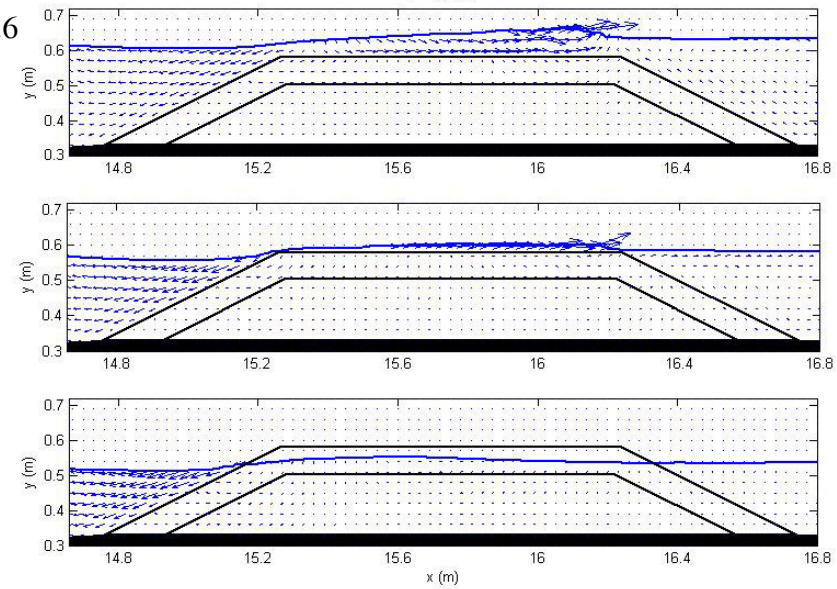

Figure 21. Snapshots of velocity field:
(a) t/T=0.0, (b) t/T=0.2, (c) t/T=0.4, (d) t/T=0.7.

When the structure is emerged, the mean flow pattern is very different. A vortex is formed leeward, but its dimensions are reduced with respect to the other tested depths. This cell is not associated with overtopping but with transmission through the structure. On the seaward slope the mean flow shows a rather complex structure, governed by the breaking conditions. Wave surging on the slope allows a greater penetration of the flow inside the porous media, and higher velocities are observed in the armour layer and the core of the seaward part of the structure. A mean current is formed in the offshore direction. In the transmission zone the onshore mean current is considerably reduced in comparison with the previous tested water depths. Even if some of these features are similar to those described for emerged vertical porous structures by Losada *et al.* (1998) using second order potential flow theory, the present model is able to show the effects of the structure slope and of wave breaking on the mean flows, substantially improving previous existing works.

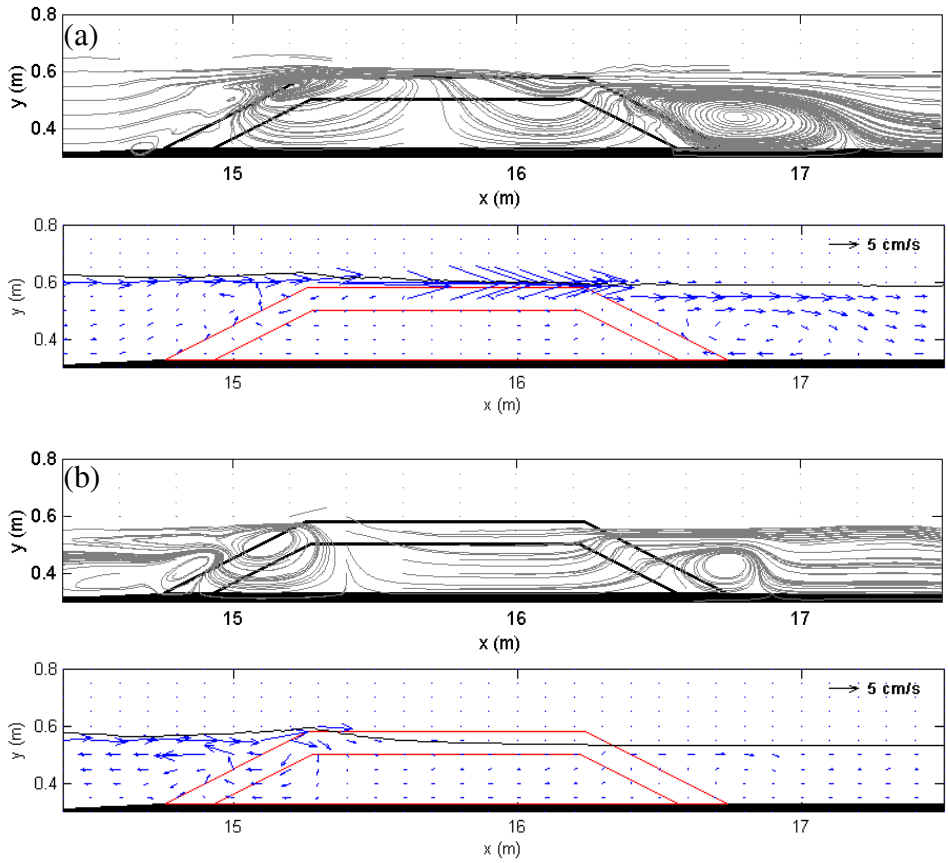

Figure 22. Computed mean (ensemble averaged) flow.
Structure freeboard (a) F=0 cm, (b) F=5 cm.

The spatial evolution of the mean flow pattern along the flume is more apparent in Figure 22 which shows the vertical distribution of the ensemble-averaged velocities at different sections of the flume. In both F = 0 and F = 5 cm configurations, the vortices give rise to an inversion of the mean flow in the water column at sections 5 and 6 corresponding to the seaward slope. At section 5 the profile is rather complex, with a shoreward component above the trough level, a seaward component below and a shoreward component at the interface with the structure. As commented above, when the structure is emerged, higher velocities are reached inside the porous media and a significant mean current directed offshore can be observed in the armour layer at section 5. This mean current is reduced at section 6. The mean flow profile is more uniform at the other sections. The reduction of the mean current in the transmission zone with the reduction of the structure freeboard can be clearly observed at section 11.

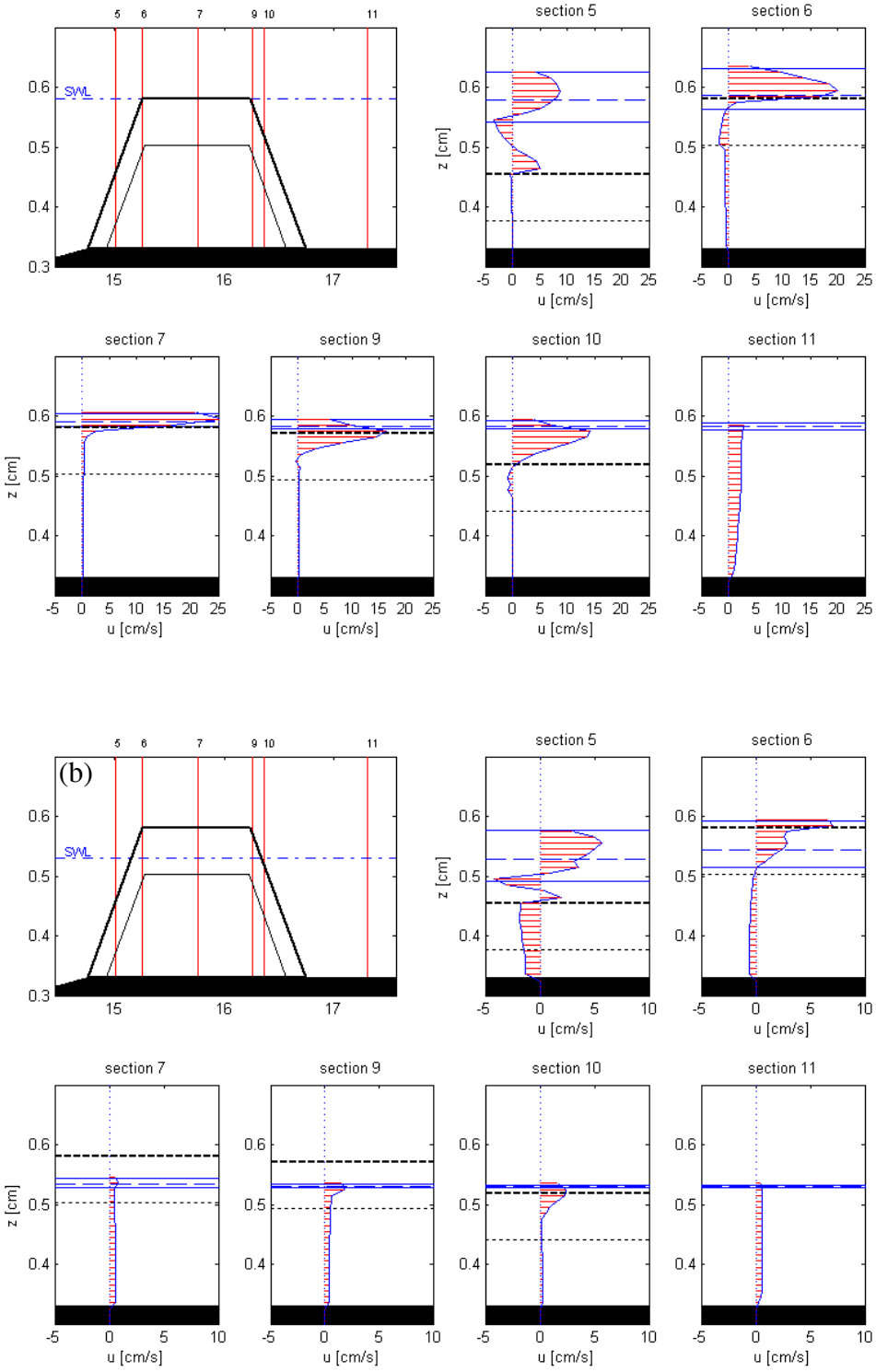

Figure 23. Computed mean (ensemble averaged) velocity profiles. Structure freeboard (a) F=0 cm, (b) F=5 cm.

5.4. Influence of the structure crest width

The width of the breakwater crest is a key parameter in the functional design of a low-crested coastal defence structure, as it determines to a large extent the structure performance in terms of energy dissipation and transmission. The same level of performance can be achieved with different combinations of structure freeboard and crest width. In particular, in coastal zones with strong aesthetics constraints a wide-crested slightly submerged structure can be preferred to a short-crested emerged structure with a similar rate of transmission. The crest width affects the mode of energy dissipation at the structure, and a combination of experimental and numerical results are used here again to study the effect of a variation of the crest with on wave breaking-induced near-field flow pattern.

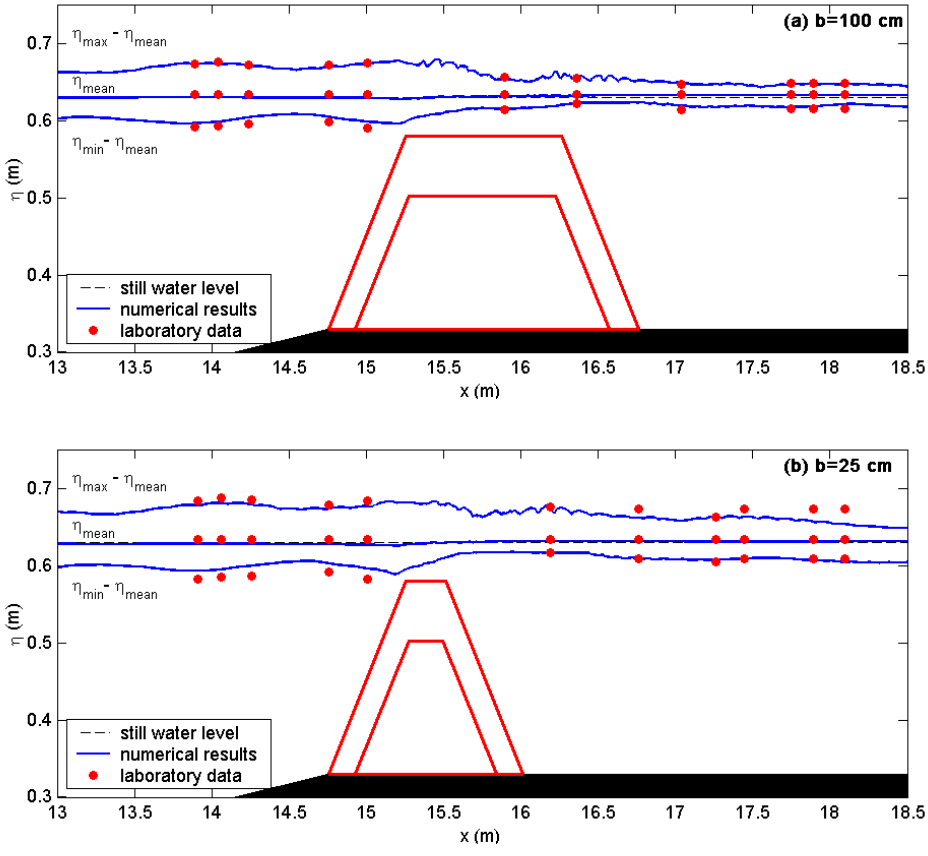

Figure 24. Wave height envelopes and mean water level, target wave conditions: h = 40 cm, T = 1.6 s, H = 10 cm.

Figure 24 presents the comparison between calculated (solid lines) and measured (dots) wave height envelopes and mean water level for both wide- and short-crested

breakwaters. As can be observed, the wave height evolution pattern along the flume is accurately captured by the numerical model in both cases. The wave height decay resulting from energy dissipation by breaking over the breakwater and friction inside the porous structure is well reproduced. Wave height envelopes show a clear quasi-standing wave pattern seaward of the structure due to reflection at the rising face of the breakwater. The reduction of wave height is clearly more pronounced in the case of the wide crest. Wave breaking occurs in both cases over the crest, just past the outer edge. In the case of the wide-crested structure, the broken wave propagates over about 75 cm in the shallow waters of the crest region, with great interaction of the breaking-induced flow with the solid skeleton of the armour layer. In the case of the short-crested structure, the broken wave immediately encounters the deeper waters of the transmission zone, with no interaction with the porous obstacle. The submerged structure induces the deformation and posterior breaking of the incident wave, but has a poor influence on the post-breaking flow conditions.

The evolution of the wave height along the flume can be observed on Figure 24 where the time series of free surface displacement recorded by the gauges located in the vicinity of the structure are presented. The high level of agreement of the computed series with the measurements should be stood out, in terms of amplitude and shape of the wave profile, for each one of the stations at the seaside, on the crest and at the leeside of the breakwater. Wave shoaling and the gradual loss of symmetry of the wave profile is correctly reproduced, as well as the broken wave profile (Figure 24a, WG6). The complex wave field leeward of the crest, with the multiple crests associated with the higher harmonics release in the deeper waters of the transmission zone, is accurately simulated. A comparison of the WG8 records shows the difference of transmitted wave height. A spectral analysis of both records establishes that the first harmonic amplitude at WG8 is 30% of the first harmonic amplitude at WG 4 in the case of the b = 100 cm structure, while it is more than 55 % for the b = 25 cm one. For the same value of structure freeboard (in that case, F = - 5 cm), the short-crested breakwater is confirmed to be less efficient as a wave load dissipator.

With regards to velocity, the numerical information is validated using the measurements realized on the seaside slope of the structure, as presented on Figure 25. The first row displays the location of the measurements points, distributed in three profiles. The wave

height envelopes and mean water level are also represented, the same way as on Figure 24. The second and third rows of the two figures show the maximum, mean and minimum profiles of phase-averaged horizontal and vertical velocities respectively. After the simulation has reached a quasi-steady state, results have been obtain based on a phase averaging of a significant number of waves. In the present case of numerical simulations including the flow recirculation system, a minimum of 50 s of simulation is needed to ensure quasi-steady conditions of flow. As can be seen on the figure, the agreement between experimental and numerical data is rather good. In the case of the wide-crested structure simulation, calibrated regarding to free surface elevation, the maximum velocities are calculated with an error between 0 and 7 %. The flow is fundamentally horizontal, with maximum horizontal velocities on an average more than three times higher than maximum vertical velocities.

Higher discrepancies exist in the case of the short crest. Many reasons may account for these differences. As mentioned earlier, the porous flow parameters were kept constant for the whole set of simulations of submerged breakwaters in order to test the reliability of the numerical model as a predictive tool. Better fits would be obtained adjusting the porous flow parameters to each case of wave conditions and structure geometry. Besides, the highest discrepancies are observed near the boundary. This may be due to the local effect of a stone of the armour layer or the presence of impurities at the bottom of the water column perturbing the measurement with laser velocimetry technique. Finally a decisive shortcoming in the computation of near-boundaries velocities should be the differences in the geometrical definition of the breakwater. The geometric configuration of the physical model is not exactly reproduced in the computational mesh: the boundaries of the porous structure as defined in the numerical flume must be regarded as an approximation of the tested rubble mound. Excluding the closest point from the boundary for all the profiles of measurements, the maximum error in the maximum horizontal velocities estimation is about 10 %.

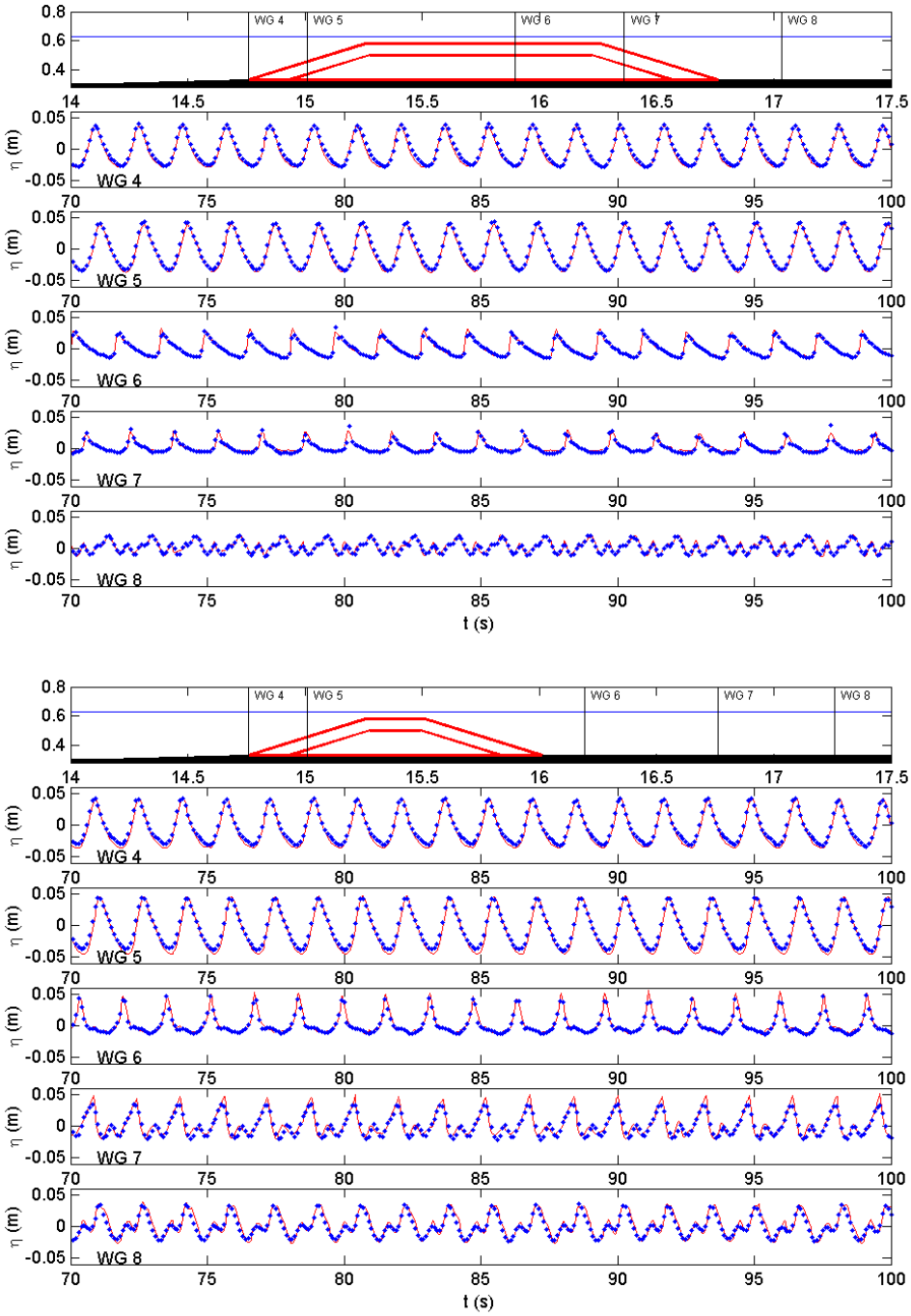

Figure 25. Free surface time series, gauges 4 to 8.
target wave conditions: h = 40 cm, T = 1.6 s, H = 10 cm.
Solid lines: experimental data. Dots: numerical results.

The velocity profiles, in terms of magnitude and shape, are, as expected, very similar on the seaside slope of the breakwater for both types of geometry. Figure 26 presents the equivalent computed velocity profiles at the leeside slope of the breakwater, for both

widths of crest. As a consequence of the higher height of the transmitted wave in the case of the short-crested breakwater, the computed values of velocities are higher, in particular the maximum horizontal velocities near the boundary in the upper part of the slope. The peak values of horizontal velocities above the trough level differ substantially. In the case of the b = 0.25 m crest width, the peak values, associated to the breaking-induced strong landward flux originated over the crest, are 1, 0.9 and 0.5 m/s at sections 1, 2 and 3 respectively, while they do not exceed 45 cm/s for the large-crested structure where incident energy is yet rather dissipated at the leeside slope. These peak values for the b = 0.25 m case do not appear on the figure, as the graph scale has been maintained for an easier global comparison. Below the crest level, the velocity profiles at the upper part of the slope show different shape. In the case of the wide-crested structure, the tendency is rather simple, from the net positive horizontal velocities near the surface to an oscillatory movement of particles near the boundary. In the case of the short-crested structure, the profile shape in the upper part of the slope is more complex, affected by breaking-induced vortex structures as will be shown further. As a consequence of the lesser energy dissipation in the crest region in the case of the short-crested structure, the inner part of the crest and the upper part of the leeside slope are affected by high values of maximum velocity intensity.

Figure 27 presents the spatial distribution of the maximum values of velocity intensity, with peak values near the surface, corresponding to wave breaking and posterior propagation of the broken wave, and local secondary peaks at the interface of the structure. The location of peak values of velocity intensity at the free surface can thus be regarded as a numerical criterion for identification of the breaking point, located in the present simulations near the x = 15.5 m horizontal coordinate for both cases. The near-field pattern of velocity evidences the differences in the post-breaking flow conditions between the two geometries of breakwater. In Figure 27a the propagation of the bore all along the crest can be observed , till the wave reforms in the transmission zone, and the pre-breaking peak at the outer edge of the crest due to the overshooting effect.

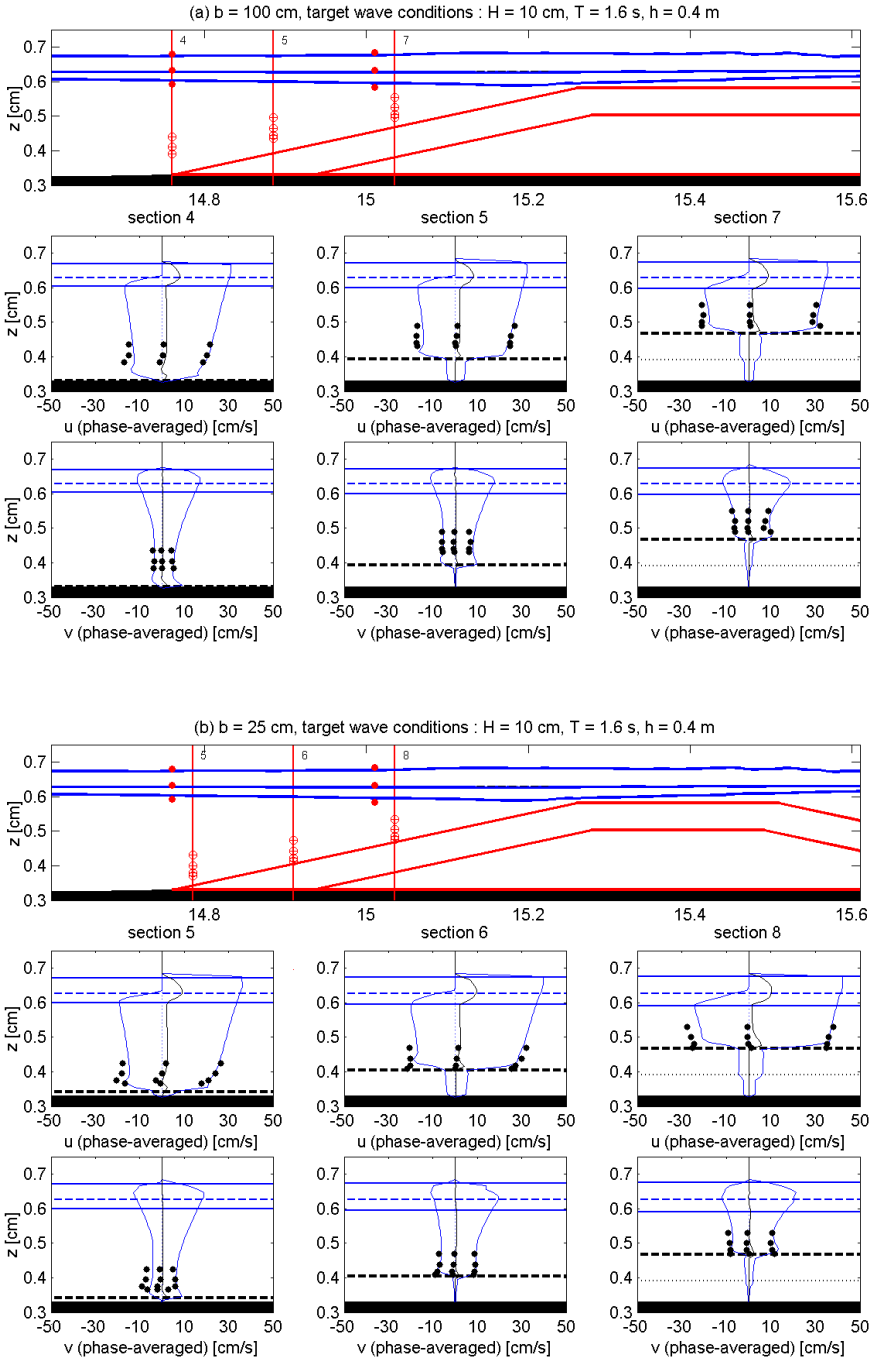

Figure 26. Phase-averaged velocity profiles at seaside slope, Solid lines: experimental data. Dashed lines: numerical results.

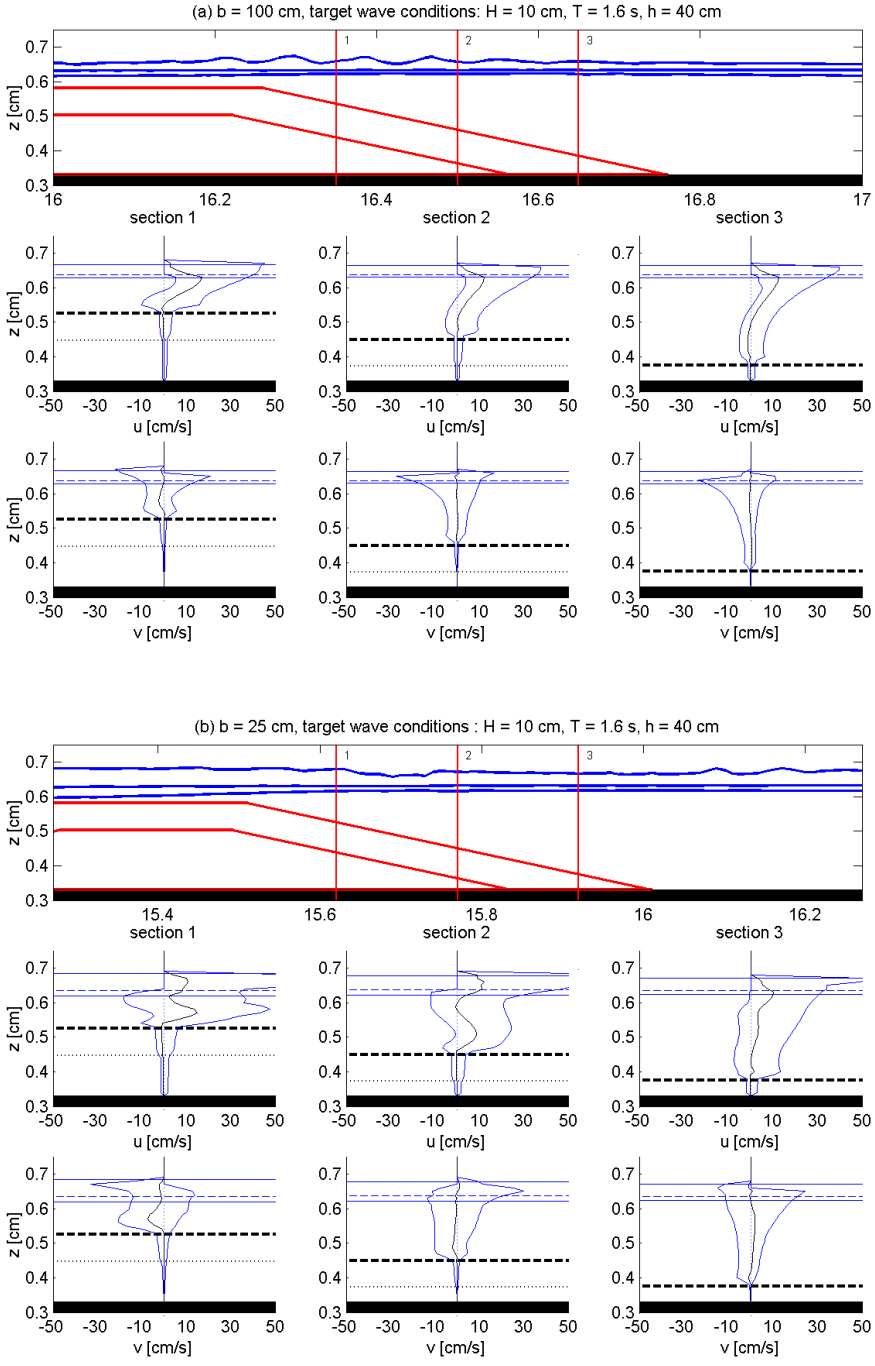

Figure 27. Computed phase-averaged velocity profiles at leeside slope.

The b = 0.25 m case map of velocity intensity allows a better visualization of the local maxima at the inner edge of the crest and upper part of the leeside slope commented earlier. Such a map provides information on the potential vulnerability of the different zones of the structure, with armour stones in the case of the short-crested structure seen to be more likely to move downward.

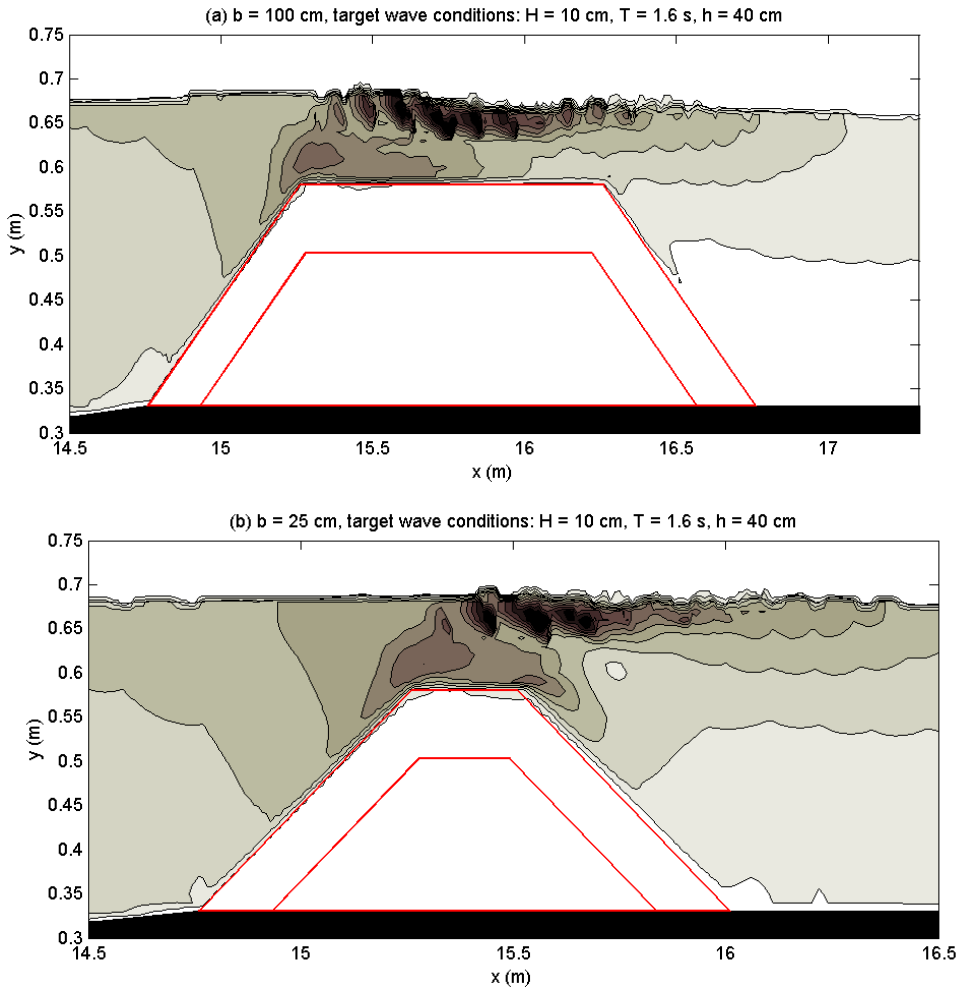

Figure 28. Computed time-averaged maximum velocity field.

Using the velocity data provided by the COBRAS model an analysis of the time-averaged mean flow around the breakwater has been carried out. Figure 28 presents the variations in the mean flow pattern at the lee side of both wide- and short-crested structures. The current pattern is very similar to what can be observed in a real situation of overtopped porous breakwater, with a strong onshore current above the crest due to flow constriction and wave breaking and formation of vortex cells leeward of the structure. This nature-like hydrodynamic behaviour is made possible by the presence of the flow recirculation system, included in both experimental and numerical wave flume and described in sections 2 and 3 of the present paper. Low-crested structures are by definition strongly overtopped structures. Overtopping produces a level set-up leeward of the structure that gives rise in real beaches to 3-D current systems. In 2-D configurations the structure overtopping results in a water piling-up in the transmission zone (see Loveless *et al.*, 1998) that heavily affects the flow conditions near the

submerged structure (Garcia *et al.*, 2003). The flow recirculation mechanism is essentially aimed to prevent such a water piling-up and to allow realistic conditions of flow at the low-crested structure. As can be seen on the figure, the mean velocities at the leeside slope of the short-crested breakwater differ

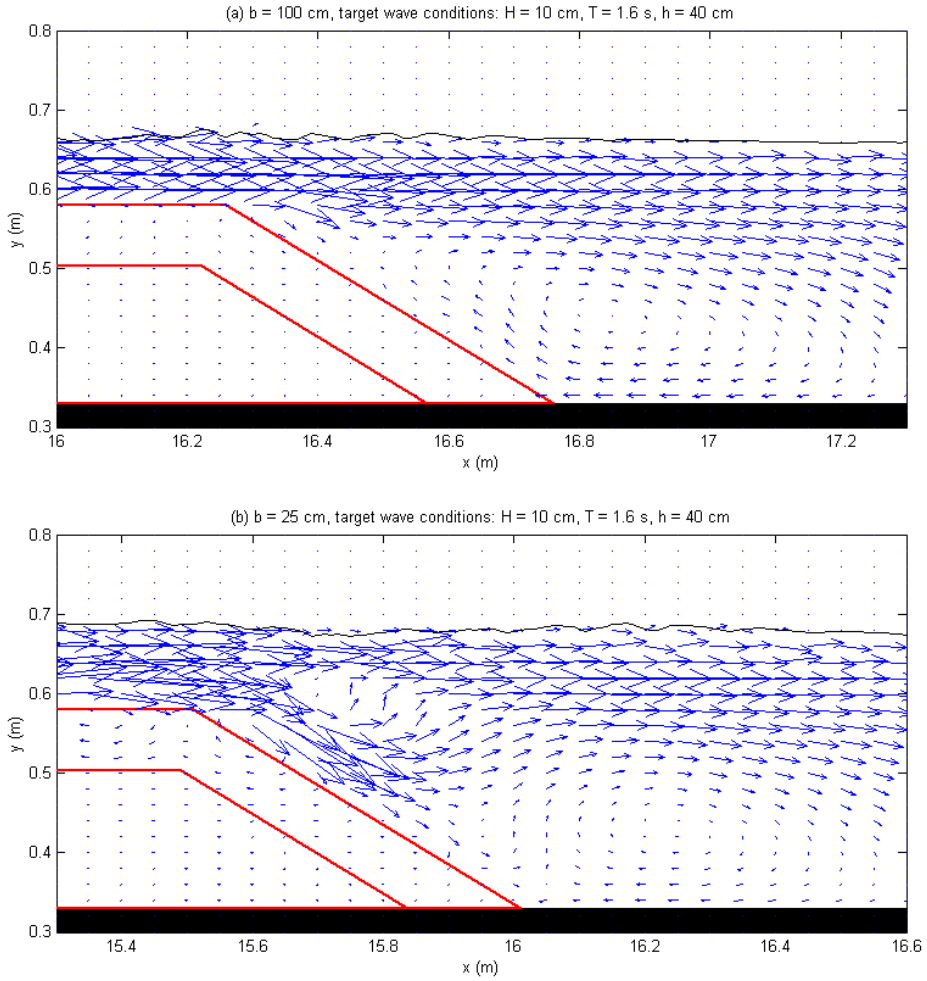

Figure 29. Computed time-averaged velocity field.

substantially from the wide crest geometry pattern. High values of mean velocities, directed downslope, can be observed in the higher middle part of the slope, with the subsequent effects on rocks stability and marine communities settlement.

6. Conclusions

In this work the physical processes associated with near-field flow-structure interaction are investigated using a numerical model based on volume-averaging of RANS equations and corresponding k-ε equations.

A series of 2DV laboratory experiments were performed in order to calibrate and validate the model. The tested structure is a porous two-layer low-crested breakwater. Different wave conditions and water depths are considered. Submerged, zero freeboard and emerged breakwaters are tested. A flow recirculation system is included to prevent non-realistic set-up leeward of the structure.

The model is proven to reproduce with a high degree of agreement the free surface displacement in the vicinity of the structure, the pressure field inside the rubble and the velocities on the seaward slope. The shoaling and breaking effects in the seaward and crest zones, as well as the higher harmonics generation phenomenon in the transmission zone, are well simulated, whether the structure freeboard is positive, zero or negative.

The present results show that this model represents a substantial improvement in the numerical modelling of LCS since it includes many processes neglected by previously existing models. Furthermore, most of the existing models based on potential theory and vertically integrated equations are able to accurately predict the free surface evolution, including breaking, but fail to give a good description of the velocity fields.

The flow recirculation system is found to deeply influence the wave height envelope patterns, the breaking conditions and the mean velocity field. The no-recirculation test simulation shows a net transport directed seaward, with very low values of the mean velocities in the transmission zone. In the recirculation case, a strong shoreward flow including a vortex cell at the lee of the structure is observed.

The influence of the structure freeboard on the near-field flow is also studied. Comparison of free surface time series along the flume and results of harmonics amplitude evolution illustrate the drastic reduction of the wave height. Numerical

breaking and mean flow patterns are presented. The model capacity in reproducing the flow conditions at a structure with a crown elevation at the still water level is outlined.

The model is proven to be a powerful tool in examining the near-field flow characteristics around low-crested structures. The data provided by the model are proven to be valid and thus can be used as an extension of the experimental data base. Numerical information can be used to study physical magnitudes difficult or impossible to measure in the laboratory, such as particle velocity above the structure crest in wave breaking conditions or flow inside the porous media.

References

Beji, S., Battjes, J.A., 1993. Experimental investigation of nonlinear wave propagation over a bar. Coastal Engineering, 19: 151-162.

Beji, S., Battjes, J.A., 1994. Numerical simulation of nonlinear wave propagation over a bar. Coastal Engineering, 23: 1-16.

Burcharth, H.F., Andersen, O.H., 1995. On the one-dimensional steady and unsteady porous flow equations. Coastal Engineering, 24: 233-257.

Chorin, A.J., 1968. Numerical solution of the Navier-Stokes equations. Mathematics of Computation, 22: 745-762.

D'Angremond, K., van der Meer, J.W., De Jong, R.J., 1996. Wave transmission at low-crested structures. Proc. 25th Int. Coastal Eng. Conf., pp. 2418-2427.

Dalrymple, R.A., Losada, M.A., Martín, P.A., 1991. Reflection and transmission from porous structures under oblique wave attack. J. Fluid Mech., 224: 625-644.

Dattatri, J., Raman, H., Jothi Shankar, N., 1978. Performance characteristics of submerged breakwaters. Proc. 16th Int. Coastal Eng. Conf., pp. 2153-2171.

Davies, B.L., Kriebel, D.L., 1992. Model testing of wave transmission past low-crested breakwaters. Proc. 23rd Int. Coastal Eng. Conf., pp. 1115-1128.

Dick, T.M., Brebner, A., 1968. Solid and permeable breakwaters. Proc. 11th Int. Coastal Eng. Conf., pp. 2153-2171.

Diskin, M.H., Vajda, M.L., Amir, I., 1970. Piling-up behind low and submerged permeable breakwaters. Journal of the Waterways, Harbors and Coastal Engineering Di Drei, E. and Lamberti, A. (2000). "Wave pumping effect of a submerged barrier." *Proc. Coastal Structures'99*, 667-673. vision, 96: 359-372.

Driscoll A.M., Dalrymple, R.A., Grilli, S.T., 1993. Harmonic generation and transmission past a submerged rectangular obstacle. Proc. 23rd Int. Coastal Eng. Conf., pp. 1142-1160.

Garcia, N., Lara, J.L., Losada, I.J. (2003). "2-D Numerical analysis of near-field flow at low-crested permeable breakwaters." *Coastal Engineering*. Submitted.

Gu, Z.G., Wang, H., 1992. Numerical modelling of wave energy dissipation within porous submerged breakwaters of irregular cross cross section. 23rd Int. Coastal Eng. Conf., pp. 1189-1202.

Hattori, M., Sakai, H., 1994. Wave breaking over permeable submerged breakwaters. Proc. 24th Int. Coastal Eng. Conf., pp. 1101-1114.

Hirt, C.W., Nichols, B.D., 1981. Volume of Fluid (VOF) method for dynamics of free boundaries. Journal of Computational Physic, 39: 201-225.

Hsu, T.-J., Sakakiyama, T., Liu, P.L.-F., 2002. A numerical model for wave motions and turbulence flows in front of a composite breakwater. Coastal Engineering, 46: 25-50.

Hur, D.-S., Mizutani, N., 2003. Numerical estimation of wave forces acting on a three-dimensional body on submerged breakwater. Coastal Engineering, 47: 329-345.

Israeli, M., Orszag, S.A., 1981. Approximation of radiation boundary conditions. Journal of Computational Physics, 41: 115-131.

Iwata, K., Kawasaki, K., Kim D.S., 1996. Breaking limit, breaking and post-breaking wave deformation due to submerged structures. Proc. 25th Int. Coastal Eng. Conf., pp. 2338-2351.

Kobayashi, N., Wurjanto, A., 1989. Wave transmission over submerged breakwaters. Journal of Waterways, Port, Coastal and Ocean Engineering, 115: 662-680.

Kothe, D.B., Mjolness, R.C., Torrey, M.D., 1991. RIPPLE: a computer program for incompressible flows with free surface. Los Alamos National Laboratory, LA-12007-MS.

Lara, J.L., 2002. Análisis experimental y numérico de los procesos asociados a la rotura sobre lechos permeables. PhD. Thesis, University of Cantabria.

Lara J.L., Losada, I.J., Liu, P.L., 2003. Breaking waves on a gravel slope. Part 1: Time averaged characteristics. Journal of Fluid Mechanics. Submitted.

Lin, P., 1998. Numerical modeling of breaking waves. Ph.D. Thesis. Cornell University.

Lin, P., Liu, P.L.-F., 1998. A numerical study of breaking waves in the surf zone. Journal of Fluid Mechanics, 359: 239-264.

Lin, P., Liu, P.L.-F., 1999. Internal wave-maker for Navier-Stokes equations models. Journal of Waterways, Port, Coastal and Ocean Engineering, 125: 207-217.

Liu, P.L.-F., Lin, P., Chang, K.A., Sakakiyama, T., 1999. Numerical modeling of wave interaction with porous structures. J. Waterway, Port, Coastal and Ocean Engineering, 125: 322-330.

Liu, P.L.-F, Lin, P., Hsu, T., Chang, K., Losada, I.J., Vidal, C., Sakakiyama, T., 2000. A Reynolds averaged Navier-Stokes equation model for nonlinear water wave and structure interactions. Proc. Coastal Structures '00, pp. 169-174.

Lomonaco, P., Vidal, C., Revilla, J.A., Losada, I.J., 2002. Flow and pressure distribution around rubble mound protected pipelines. Proc. 2nd International Conference on Marine Waste Water Discharges.

Losada, I.J., Dalrymple, R.A., Losada, M., 1993. Water waves on crown breakwaters. Journal of Waterways, Port, Coastal and Ocean Engineering, 119: 367-380.

Losada, I.J., Silva, R., Losada, M.A., 1996a. 3-D non-breaking regular wave interaction with submerged breakwaters. Coastal Engineering, 28: 229-248.

Losada I.J, Silva, R., Losada, M.A., 1996b. Interaction of non-breaking directional random waves with submerged breakwaters. Coastal Engineering, 28: 249-266.

Losada I.J, Patterson, M., Losada, M.A., 1997. Harmonic generation past a submerged porous step. Coastal Engineering, 31: 281-304.

Losada, I.J., Dalrymple, M.A., Losada, M.A., 1998. Wave-induced mean flows in vertical rubble-mound structures. Coastal Engineering 31: 251-281.

Loveless, J., Debski, D., 1997. Wave transmission and set-up at detached breakwaters. Proc. Coastal Dynamics '97: 674-683.

Loveless, J., Debski, D., MacLeod, A.B., 1998. Sea level set-up behind detached breakwaters. Proc. 26th Int. Coastal Eng. Conf., pp. 1665-1678.

Madsen, O.S., White, S.M., 1976. Wave transmission through trapezoidal breakwaters. Proc. 15th Int. Coastal Eng. Conf., pp. 2662-2676.

Massel, S., Butowski, P., 1980. Wind waves transmission through porous breakwater. Proc. 16th Int. Coastal Eng. Conf., pp. 333-346.

Masselink, G., 1998. Field investigation of wave propagation over a bar and the consequent generation of secondary waves. Coastal Engineering 33: 1-9.

Ohyama, T., Nadaoka, K., 1992. Modeling the transformation of nonlinear waves passing over a submerged dike. 23rd Int. Coastal Eng. Conf., pp. 526-539.

Petit, H.A.H., Bosch, P. van den, Gent, M.R.A. van, 1994a. SKYLLA: wave motion in and on coastal structures; implementation and verification of modified boundaries. conditions. Delft Hydraulics Report H1780.

Petit, H.A.H., Bosch, P. van den, Gent, M.R.A. van, 1994b. SKYLLA: wave motion in and on coastal structures; implementation of impermeable slope and overtopping-boundary conditions. Delft Hydraulics Report H1780.

Rojanakamthorn, S., Isobe, M., Watanabe, A., 1989. A mathematical model of wave transformation over a submerged breakwater. Coastal Engineering in Japan, 32: 209-234.

Rojanakamthorn, S., Isobe, M., Watanabe, A., 1990. Modeling of wave transformation on submerged breakwater. Proc. 22nd Int. Coastal Eng. Conf., pp. 1060-1073.

Seabrook, S.R., Hall, K.R., 1998. Wave transmission at submerged rubblemound breakwaters. Proc. 26th Int. Coastal Eng. Conf., pp. 2000-2013.

Seelig, W.N., 1980. Two-dimensional test of wave transmission and reflection characteristics of laboratory breakwaters. Technical report No.80-1, U.S. Army Coastal Eng. Res. Center, Fort Belvoir, VA.

Sénéchal, N., Bonneton, P., Dupuis, H., 2002. Field experiment on secondary wave generation on a barred beach and the consequent evolution of energy dissipation on the beach face. Coastal Engineering 46: 233-247.

Shih, R.W.K., 1990. Permeability characteristics of rubble material – New formulae. Proc. 22nd Int. Coastal Eng. Conf., pp. 1499-1512.

Sollit, C.K., Cross, R.H., 1972. Wave reflection and transmission at permeable breakwaters. Technical report No. 147, R.M. Parsons Lab., Dept of Civil Eng., MIT.

Troch, P., de Rouck, J., 1998. Development of two-dimensional numerical wave flume for wave interaction with rubble mound breakwaters. 26th Int. Coastal Eng. Conf., pp. 1638-1649.

Van der Meer, J.W., Petit, H.A.H., Bosh, P. van den, Klopman, G., Broekens, R.D., 1992. Numerical simulation of wave motion on and in coastal structures. 23rd Int. Coastal Eng. Conf., pp. 1772-1784.

Van Gent, M.R.A., 1994. The modelling of wave action on and in coastal structures. Coastal Engineering, 22: 311-339.

Van Gent, M.R.A., 1995. Porous flow through rubble-mound material. Journal of Waterway, Port, Coastal and Ocean Engineering, 121: 176-181.

Van Gent, M.R.A., Tönjes, P., Petit, A., van den Bosch, P., 1994. Wave action on and in permeable structures. Proc. 24th Int. Coastal Eng. Conf., pp. 1739-1753.

Vidal, C., Lomónaco, P., Migoya, L., Archetti, R., Turchetti, M., Sorci, M., Sassi, G., 2001. Laboratory experiments on flow around and inside LCS structures. Description of tests and data base. DELOS European Project, technical report.

Wibbeler, H., Oumeraci, H., 1992. Finite element simulation of wave-induced internal flow in rubble mound structures. Proc. 23rd Int. Coastal Eng. Conf., pp.1707-1719.

LIST OF FIGURES